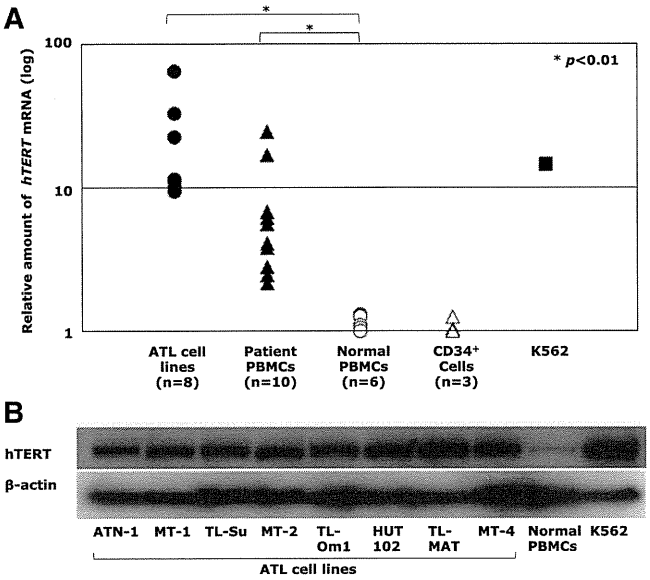

Figure 1. Abundant expression of hTERT in ATL tumor cells. (A) Expression of *hTERT* mRNA in ATL/HTLV-I infected cell lines (■), freshly isolated ATL tumor cells from patients (▲), normal PBMCs (○), and CB-CD34$^+$ cells (△) were examined by qRT-PCR. The level of *hTERT* mRNA expression in the K562 leukemia cell line (●) was used as an internal control. The expression level of *hTERT* mRNA in each sample was calculated relative to that of PBMCs. *hTERT* mRNA expression relative to normal PBMCs was 21.3 ± 17.9 for the ATL/HTLV-I–infected cell line, 7.48 ± 6.89 for freshly isolated ATL tumor cells, and 1.10 ± 0.12 for CB-CD34$^+$ (mean ± standard deviation [SD]). The ATL/HTLV-I–infected cell line and freshly isolated ATL tumor cells expressed *hTERT* mRNA abundantly and significantly (*$P < .01$). (B) Expression of hTERT protein in ATL cell lines and normal PBMCs was confirmed by western blotting.

Western blotting of hTERT protein

For analysis of protein expression, western blotting was performed as described previously.[35] Briefly, cell lysates were subjected to 10% sodium dodecyl sulfate polyacrylamide gel electrophoresis (e-PAGEL, ATTO) and blotted onto polyvinylidene difluoride membranes (Bio-Rad Laboratories). The blots were incubated first with anti-hTERT rabbit mAb (Millipore), then with horseradish peroxidase–conjugated anti-rabbit immunoglobulin G Ab (GE Healthcare). The probed proteins were visualized by using an enhanced chemiluminescence system (GE Healthcare). Subsequently, the blotted membranes were stripped and reprobed with anti–β-actin mouse mAb (Sigma-Aldrich) to confirm equivalent protein loading between samples.

Detection of hTERT$_{461\text{-}469}$–specific CTL precursors in the periphery of ATL patients

PBMCs from HLA-A*24:02$^+$, HLA-A*24:02$^-$ ATL patients, or HLA-A*24:02$^+$ healthy individuals were seeded in 24-well plates at 1.5 × 10^6 per well in the presence of the hTERT$_{461\text{-}469}$ peptide at a concentration of 1 μM in GT-T503 medium supplemented with 5% human serum and 10 U/mL IL-2. After culturing for 14 days, cultured PBMCs were stained with FITC-conjugated anti-CD8 mAb and HLA-A*24:02/hTERT$_{461\text{-}469}$ tetramer or control tetramer at a concentration of 20 μg/mL at 4°C for 20 minutes. Subsequently, the stained cells were analyzed by flow cytometry.

IFN-γ secretion assay

hTERT-*siTCR*/CD8 or K3-1 (2 × 10^4) cells were incubated with 2 × 10^4 hTERT$_{461\text{-}469}$ peptide-pulsed (1 μM) or unpulsed K562-A24 or K562 cells for 24 hours. Interferon gamma (IFN-γ) in the culture supernatant was measured by using an enzyme-linked immunosorbent assay kit (Pierce). Enzyme-linked immunospot assays were used to detect the epitope-responsive IFN-γ production mediated by hTERT$_{461\text{-}469}$-specific CTL precursors in the periphery of ATL patients as described previously.[34]

Anti-ATL tumor effect of hTERT-*siTCR*–transduced CD8$^+$ T cells in xenografted mouse models

To assess the in vivo anti-ATL tumor effect mediated by hTERT-*siTCR*/CD8, a bioluminescence assay using a xenografted mouse model was used. First, we lentivirally generated a luciferase gene–transduced HLA-A*24:02$^+$ ATL cell line, ATN-1 (ATN-1/luc). For measurement, anesthetized xenografted mice were given an intraperitoneal injection of 2.5 mg/body VivoGlo luciferin (Caliper Life Science), and images were acquired for 5 to 10 minutes by using an AEQUORIA luminescence imaging system (Hamamatsu Photonics). The acquired photon counts were analyzed by using AQUACOSMOS software (Hamamatsu Photonics).

Six-week-old NOD/scid/γc^{null} (NOG) female mice[37] were purchased from the Central Institute for Experimental Animals and maintained in the institutional animal facility at Ehime University. All in vivo experiments were approved by the Ehime University animal care committee. For the Winn assay, 5 × 10^5 ATN-1/luc cells and 2.5 × 10^6 hTERT-*siTCR*/CD8 or non–gene-modified CD8$^+$ T cells (NGM/CD8) were subcutaneously inoculated into the abdominal wall of NOG mice that had been pretreated with 1 Gy irradiation. Thereafter, 2.5 × 10^6 effector cells of each type were administered weekly to the corresponding mice, respectively, via the tail vein for a total of 3 times. For the adoptive transfer experiments, similarly pretreated mice were intravenously inoculated with 5 × 10^5 ATN-1/luc cells. After 4 days, mice started to receive intravenously infused 5 × 10^6 hTERT-*siTCR*/CD8 or NGM/CD8, respectively, for a total of 5 times. These mice were serially monitored for tumor growth determined by photon counts acquired every 7 days until they were euthanized owing to disease progression.

Statistical analysis

The Mann-Whitney *U* test was used to assess differences between two groups; a *P* value of < .05 was considered significant.

Results

ATL tumor cells abundantly express *hTERT* mRNA and hTERT protein

The expression level of *hTERT* mRNA in the ATL/HTLV-I–infected cell line (n = 8), freshly isolated tumor cells from ATL patients (n = 10), normal PBMCs from healthy individuals (n = 6), and CD34$^+$ cells from normal CBMCs (CB-CD34$^+$) (n = 3) were measured by using the qRT-PCR method. *hTERT* mRNA expression relative to normal PBMCs was 21.3 ± 17.9 for the ATL/HTLV-I–infected cell line, 7.48 ± 6.89 for freshly isolated ATL tumor cells, and 1.10 ± 0.12 for CB-CD34$^+$ cells (mean ± standard deviation). In Figure 1A, the ATL/HTLV-I–infected cell line and freshly isolated ATL tumor cells, but not CB-CD34$^+$, abundantly produced *hTERT* mRNA in comparison with normal PBMCs, the difference being statistically significant. The *P* value was .002 for the ATL/HTLV-I–infected cell line, .001 for freshly isolated ATL tumor cells, and .243 for CB-CD34$^+$ cells. Similarly, western blotting demonstrated abundant expression of hTERT protein in the ATL tumor cells (Figure 1B).

Circulatory hTERT$_{461\text{-}469}$-specific CTL precursors were exclusively detectable in the periphery of HLA-A*24:02$^+$ ATL patients

Next, by using the tetramer assay, we examined circulatory hTERT$_{461\text{-}469}$-specific CTL precursors in PBMCs from HLA-A*24:02$^+$ ATL patients (n = 7), HLA-A*24:02$^-$ ATL patients (n = 3) before chemotherapy, and HLA-A*24:02$^+$ healthy individuals as controls (n = 6). Since freshly isolated PB lymphocytes were almost

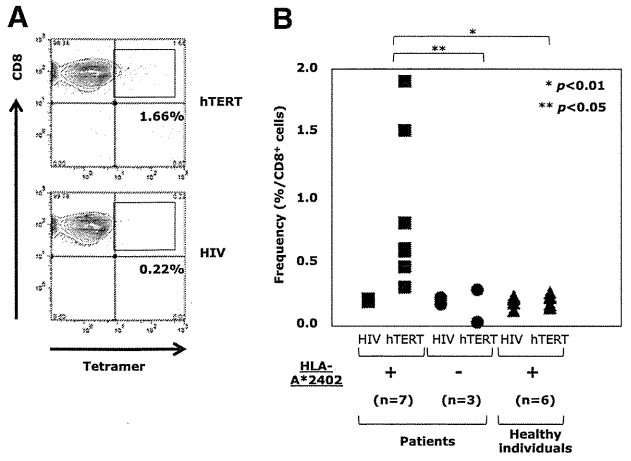

Figure 2. Detection of circulatory hTERT$_{461-469}$-specific CTL precursors in the periphery of ATL patients. (A) hTERT$_{461-469}$-specific CTL precursors in PBMCs repetitively stimulated with hTERT$_{461-469}$ peptide from HLA-A*24:02$^+$ ATL patients were detected by using HLA-A*24:02/hTERT$_{461-469}$ tetramer. A representative case is shown. HLA-A*24:02/HIV tetramer was used as a negative control. (B) In comparison with HLA-A*24:02$^-$ ATL patients (●) (n = 3) and HLA-A*24:02$^+$ healthy individuals (▲) (n = 6), the frequency of hTERT$_{461-469}$-specific CTL precursors in HLA-A*24:02$^+$ ATL patients (■) (n = 7) was significantly high (*$P < .01$; **$P < .05$). The frequency was 0.88% ± 0.55% for HLA-A*24:02$^+$ ATL patients, 0.11% ± 0.1% for HLA-A*24:02$^-$ ATL patients, and 0.2% ± 0.04% for HLA-A*24:02$^+$ healthy individuals (mean ± SD).

negative for tetramer staining, PBMCs stimulated with hTERT$_{461-469}$ peptide were analyzed. A representative example of an HLA-A*24:02$^+$ ATL patient is shown in Figure 2A. The frequencies of hTERT$_{461-469}$-specific CTL precursors in HLA-A*24:02$^+$ and HLA-A*24:02$^-$ ATL patients and HLA-A*24:02$^+$ healthy individuals are summarized in Figure 2B. hTERT$_{461-469}$-specific CTL precursors were detected at 0.88% ± 0.55% in HLA-A*24:02$^+$ ATL patients, being significantly more frequent than in HLA-A*24:02$^-$ ATL patients (0.11% ± 0.1%; $P < .05$) or HLA-A*24:02$^+$ healthy individuals (0.2% ± 0.04%; $P < .01$). These observations confirmed the presence of primed memory CD8$^+$ T cells with hTERT$_{461-469}$ epitope/HLA-A*24:02 complex (ie, that the hTERT$_{461-469}$ epitope must be naturally immunogenic) in HLA-A*24:02$^+$ ATL patients.

hTERT-*siTCR*–transduced CD8$^+$ T cells exert anti-ATL reactivity in vitro

The hTERT-*siTCR* gene was retrovirally introduced into normal CD8$^+$ T cells. Transduction efficiency determined by expression of Vβ2 on the gene-modified T cells was 85% to 95% (data not shown), and almost 50% of the transfectants were positive for HLA-A*24:02/hTERT$_{461-469}$ tetramer (Figure 3A). The cognate epitope specificity and HLA-A*24:02 restriction were examined by using standard ^{51}Cr-release assays (Figure 3B). Because expression of *hTERT* mRNA in LCLs was upregulated (supplemental Figure 2C), hTERT peptide-unpulsed HLA-A*24:02$^+$ LCLs were killed to some extent, reflecting the presence of endogenously processed hTERT (Figure 3B). Such epitope-specific cytotoxicity mediated by hTERT-*siTCR*/CD8 was obviously attenuated by anti-HLA class I mAb, but not by anti-HLA-DR mAb (Figure 3C). The antigen sensitivity to cognate hTERT$_{461-469}$ peptide mediated by hTERT-*siTCR*/CD8 (shown in Figure 3D) was similar to that of the parental CTL clone, K3-1 (Figure 3E-F).

hTERT-*siTCR*/CD8 dose-dependently killed the HLA-A*24:02$^+$ ATL/HTLV-I–infected cell lines ATN-1, TL-Su, and MT-2, but not the HLA-A*24:02$^-$ TL-Om1, HUT102, and MT-4 (Figure 4A). Additionally, the tumoricidal effect mediated by hTERT-*siTCR*/CD8 was abrogated by anti-HLA class I mAb, but not by anti-HLA-DR mAb (Figure 4B). Furthermore, time-lapse imaging directly demonstrated this tumoricidal activity of hTERT-*siTCR*/CD8 against HLA-A*24:02$^+$ ATN-1, but not that against HLA-A*24:02$^-$ HUT102 or K562 (negative control) (supplemental Fig 1-(1)). We then examined the tumoricidal activity against freshly isolated ATL tumor cells and found that these transfectants also dose-dependently killed HLA-A*24:02$^+$, but not -A*24:02$^-$ freshly isolated ATL tumor cells (Figure 5A).

Conversely, as shown in Figure 5B, neither HLA-A*24:02$^+$ normal CD4$^+$ T cells (the normal counterpart of ATL tumor cells)

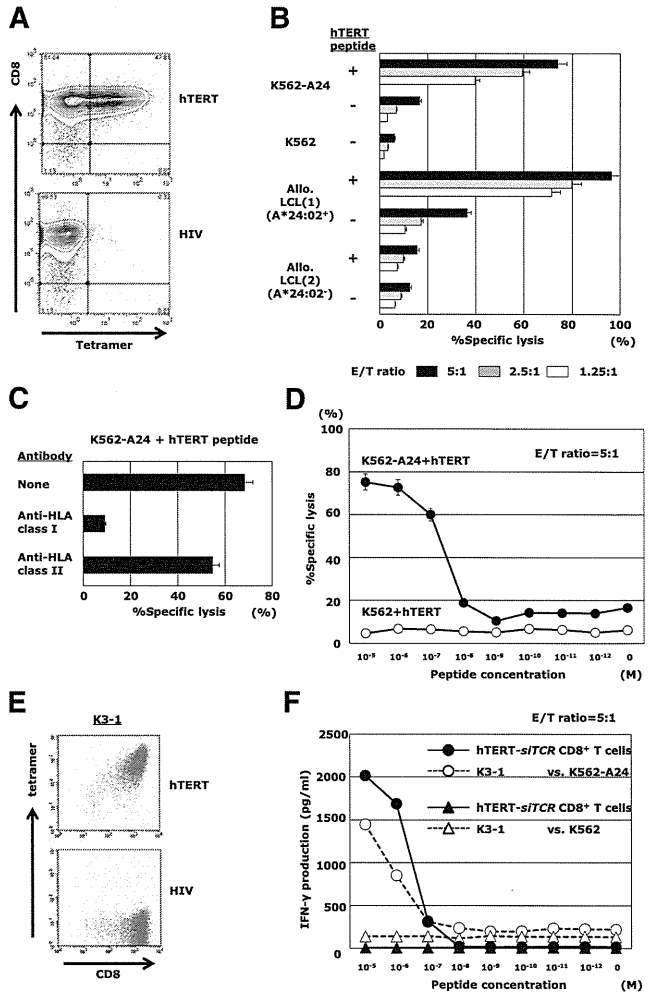

Figure 3. hTERT-*siTCR*–transduced CD8$^+$ T cells display epitope-specific responsiveness. (A) Representative flow cytometry plots showing staining of hTERT-*siTCR*–transduced CD8$^+$ T cells with HLA-A*24:02/hTERT$_{461-469}$ tetramer. HLA-A*24:02/HIV tetramer was used as a negative control. (B) ^{51}Cr-release assays were conducted by using hTERT-*siTCR*–transduced CD8$^+$ T cells with unpulsed or hTERT$_{461-469}$ peptide-loaded (1 μM) K562-A24, K562, HLA-A*24:02$^+$, or HLA-A*24:02$^-$ allogeneic B-LCLs at the indicated effector:target (E/T) ratios. (C) Effect of HLA class I and class II blockade on the cytotoxic activity of hTERT-*siTCR*–transduced CD8$^+$ T cells against the cognate peptide-pulsed (1 μM) K562-A24 was determined by ^{51}Cr-release assays at an E/T ratio of 5:1. (D) hTERT-*siTCR*–transduced CD8$^+$ T cells were tested in ^{51}Cr release assays against K562 (negative control) and K562-A24 cells pulsed with the indicated concentrations of hTERT$_{461-469}$ peptide at an E/T ratio of 5:1. Error bars represent SDs. (E) Representative flow cytometry plots showing staining of K3-1 with the HLA-A*24:02/hTERT$_{461-469}$ tetramer (upper) and the irrelevant HLA-A*24:02/HIV-1 Env$_{584-592}$ tetramer (negative control; bottom). (F) IFN-γ production by hTERT-*siTCR*–transduced CD8$^+$ T cells was measured by using a format similar to that described for panel D. The parental K3-1 CTL clone was tested in parallel.

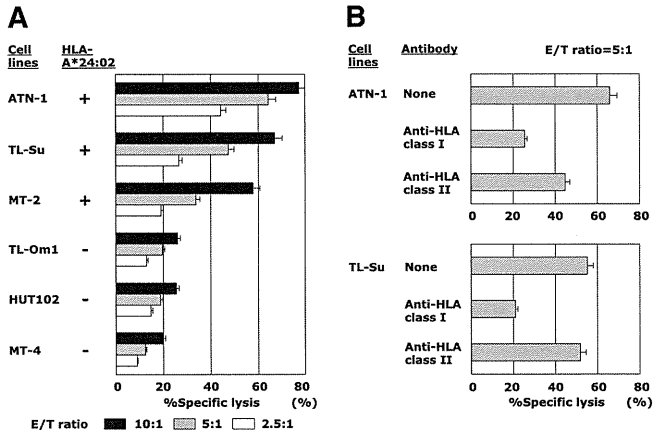

Figure 4. Cytotoxic activity of hTERT-*siTCR*–transduced CD8$^+$ T cells against ATL/HTLV-I–infected cell lines. (A) Cytotoxic activity of hTERT-*siTCR*–transduced CD8$^+$ T cells against HLA-A*24:02$^+$ or HLA-A*24:02$^-$ ATL/HTLV-I–infected cell lines was tested in ^{51}Cr-release assays at the indicated E/T ratios. All tested ATL/HTLV-I–infected cell lines overexpressed *hTERT* mRNA and protein, as shown in Figure 1. (B) Effect of HLA class I and class II blockade on the cytotoxic activity of hTERT-*siTCR*–transduced CD8$^+$ T cells against ATN-1 and TL-Su was tested in ^{51}Cr-release assays at an E/T ratio of 5:1.

nor HLA-A*24:02$^+$ normal CB-CD34$^+$ cells as normal hematopoietic progenitor cells were killed. In the same experiment, newly established IL-2–dependent HTLV-I–infected CD4$^+$ T cells (Patient #1 and Patient #2), but not the corresponding original normal/HTLV-I$^-$ CD4$^+$ T cells (Patient #1 and Patient #2), became to some extent sensitive to the same transfectants as the level of *hTERT* mRNA expression increased (Figure 5B). This observation confirmed that not only ATL tumor cells, but also HTLV-I–infected cells from which ATL tumor cells were derived could be killed by these hTERT-specific effector cells.

Next, because the majority of ATL patients were of an advanced age and were therefore ineligible for allo-HSCT, we examined the tumoricidal activity against autologous ATL tumor cells mediated by gene-modified PB-CD8$^+$ T cells from the patient (Figure 6). Although PB-CD8$^+$ T cells from heavily pretreated ATL patients were sometimes difficult to subject to *TCR* gene modification and ex vivo expansion, hTERT-*siTCR*/CD8 cells generated from HLA-A*24:02$^+$ patients (n = 3) were able to substantially lyse autologous ATL tumor cells in proportion to the corresponding level of *hTERT* mRNA expression. Autologous CD14$^+$ PB monocytes were used as a negative control because they lacked expression of *hTERT* mRNA. These results demonstrated that hTERT-*siTCR*/CD8 cells were able to exert tumoricidal activity against ATL tumor cells through recognition of the hTERT$_{461\text{-}469}$ epitope/HLA-A*24:02 complex, which is naturally presented on the surface of ATL tumor cells.

hTERT-*siTCR*–transduced CD8$^+$ T cells display in vivo anti-ATL reactivity

In vivo anti-ATL reactivity mediated by hTERT-*siTCR*/CD8 cells was assessed by using a xenografted mouse model and bioluminescence assay. Serial bioluminescence assay images were simultaneously acquired.

In the Winn assay (Figure 7A), tumor cell growth in NOG mice treated with hTERT-*siTCR*/CD8 (n = 2) was completely inhibited for longer than 6 months. In contrast, when compared with non-treated NOG mice (n = 2) in which the inoculated ATL tumor mass rapidly enlarged, activated NGM/CD8 (n = 2) did suppress ATL tumor growth to some degree, but eventually huge tumor masses developed within 2 months. In a therapeutic adoptive transfer model (Figure 7B), the tumor cell growth in mice treated with hTERT-*siTCR*/CD8 (n = 2) was obviously suppressed within the 8-week observation period, in contrast to that in mice treated with NGM/CD8 (n = 2) and that in control mice (n = 2).

Discussion

Although ATL still has a poor prognosis, the clinical presence of the graft-versus-ATL in patients treated successfully by allo-HSCT has encouraged the search for a novel cellular immune-mediated treatment of ATL. Unlike EBV-related malignancy,[6] the feasibility of HTLV-I–associated Tax[7] and HBZ[8] proteins as therapeutic targets of anti-ATL immunotherapy still remains controversial. Therefore, in this study, we explored the feasibility of a novel therapeutic target other than one associated with HTLV-I. Consequently, we demonstrated for the first time that hTERT was a promising therapeutic target for anti-ATL adoptive immunotherapy. Freshly isolated ATL tumor cells produced *hTERT* mRNA abundantly, and HLA-A*24:02-restricted and hTERT$_{461\text{-}469}$-specific CTL precursors were detected in the periphery of HLA-A*24:02$^+$ ATL patients. These findings suggested that naturally processed and presented hTERT$_{461\text{-}469}$/HLA-A*24:02 complex on the surface of ATL tumor cells was sufficiently immunogenic to be recognized by the target-specific CTLs in HLA-A*24:02$^+$ ATL patients. Additionally, *hTERT* mRNA expression in newly generated HTLV-I–infected CD4$^+$ T cells was upregulated, and these cells became sensitive to gene-modified hTERT-specific CTLs (Figure 5B). The involvement of Tax[12] and HBZ[38] in upregulation of the *hTERT* gene in

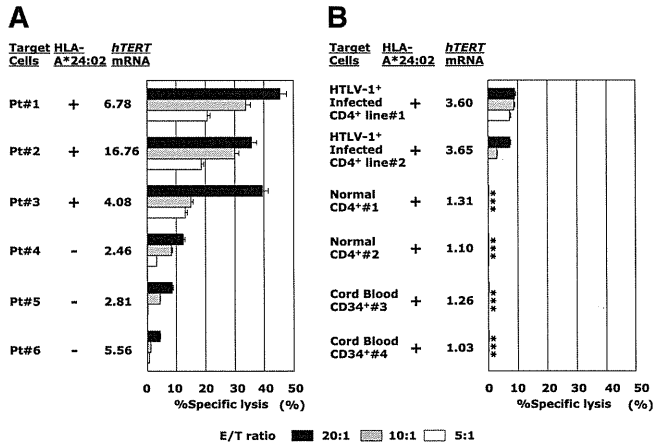

Figure 5. hTERT-*siTCR*–transduced CD8$^+$ T cells kill freshly isolated ATL cells and newly HTLV-I–infected CD4$^+$ T cells, but not normal cells, in vitro. (A) Freshly isolated HLA-A*24:02$^+$ (n = 3) or HLA-A*24:02$^-$ (n = 3) ATL tumor cells overexpressing *hTERT* mRNA were used as targets in ^{51}Cr-release assays with hTERT-*siTCR*–transduced CD8$^+$ T cells at the indicated E/T ratios. (B) The same hTERT-*siTCR*–transduced CD8$^+$ T cells used in panel A at the same E/T ratios were tested in ^{51}Cr-release assays against newly generated HLA-A*24:02$^+$ HTLV-I–infected CD4$^+$ T cells (n = 2) representing HTLV-I carrier CD4$^+$ T cells, original HLA-A*24:02$^+$ normal CD4$^+$ T cells (n = 2) representing the normal counterpart ATL tumor cells (corresponding number indicating cells from the identical donor), and HLA-A*24:02$^+$ normal CB-CD34$^+$ cells (n = 2) encompassing steady-state normal hematopoietic progenitor cells. Listed levels of expression of *hTERT* mRNA are those relative to the mean levels of expression across 6 PBMC samples from healthy donors determined by qRT-PCR and calculated by using the comparative threshold cycle method. Error bars represent SDs (* indicates less than detectable).

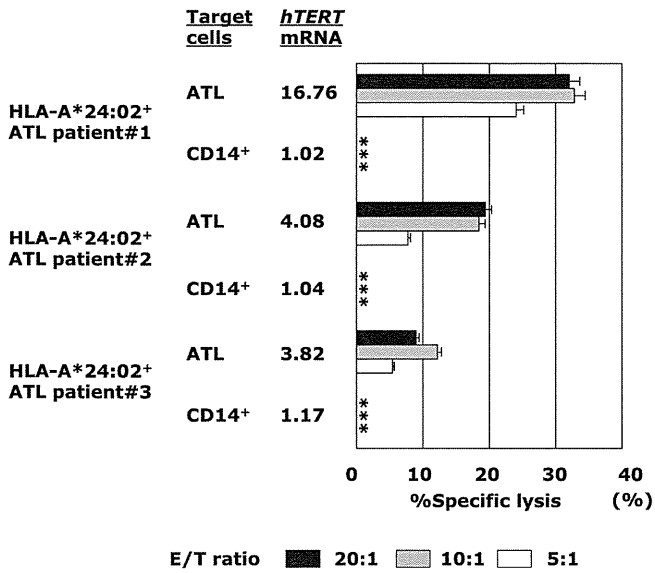

Figure 6. hTERT-*siTCR*–transduced CD8$^+$ T cells kill freshly isolated autologous ATL tumor cells on the basis of hTERT expression levels. Cytotoxic activity of hTERT-*siTCR*–transduced CD8$^+$ T cells obtained from HLA-A*24:02$^+$ ATL patients (n = 3) against autologous freshly isolated ATL tumor cells and autologous peripheral CD14$^+$ cells (negative control) was tested in ^{51}Cr-release assays at the indicated E/T ratios. *hTERT* mRNA in each patient's ATL tumor cells is listed using a format similar to that used in Figure 5. Error bars represent SDs (* indicates less than detectable).

HTLV-I–infected immortalized CD4$^+$ T cells and ATL tumor cells has been reported previously. Initially, it might seem more realistic to develop an hTERT$_{461\text{-}469}$ peptide vaccine for treatment of HLA-A*24:02$^+$ ATL patients. However, because we were concerned that CTL induction of hTERT peptide vaccine might have a tendency to be impeded by the regulatory T-cell function of ATL tumor cells,[21] we focused on developing a redirected T-cell–based adoptive immunotherapy targeting hTERT to allow administration of a number of hTERT-specific CTLs directly.

To this end, we cloned the full-length rearranged *TCR-α/β* genes from K3-1, the HLA-A*24:02-restricted and hTERT$_{461\text{-}469}$-specific CTL clone.[19] With codon optimization of the constant regions, we inserted them into our new souped-up second-generation 2A peptide-based *siTCR* vector to accomplish an increased expression level of the introduced TCR, carrying small interfering RNAs for the endogenous *TCR-α/β* genes in the redirected T cells (hTERT-*siTCR* vector).[26,27,34] The *siTCR* vector system makes it possible to simultaneously accomplish profound suppression of endogenous *TCR* genes and markedly increase the cell-surface expression of the introduced TCR, resulting in upregulated antitumor reactivity,[34] thus leading to inhibition of mispaired TCR formation between the endogenous and introduced TCR-α and -β chains, and lowering the potential risk of lethal graft-versus-host disease.[39] We found that both allogeneic and autologous gene-modified CD8$^+$ T cells using the hTERT-*siTCR* vector successfully killed ATL tumor cells both in vitro and in vivo (Figures 4-7), but not normal cells, including steady-state hematopoietic progenitor cells (Figure 5B). The introduced cytocidal activity against ATL tumor cells mediated by these gene-modified CTLs was actually accomplished through recognition of the HLA-A*24:02/hTERT$_{461\text{-}469}$ complex on the surface of ATL tumor cells (Figures 3 and 4).

Clinical studies of anticancer immunotherapy targeting hTERT have not demonstrated any significant adverse events so far.[14-17,20] However, for clinical application, because a number of activated gene-modified hTERT-specific CTLs would be administered at once, it would again be necessary to be mindful of on-target adverse events against normal tissues that constitutively express the *hTERT* gene.[10,40] Notably, any impairment of hematopoiesis would be the major concern. In this study, both allogeneic and autologous gene-modified effector CD8$^+$ T cells expressing hTERT-specific TCR from adult peripheral lymphocytes, and CB lymphocytes did not kill CB-CD34$^+$ cells representing steady-state hematopoietic progenitors (Figure 5B). By using cytokine-driven myeloid differentiation with CB-CD34$^+$ cells, gene-modified CTLs targeting hTERT showed a slight cytocidal effect against differentiated and highly proliferating subsets of CD34$^+$CD33$^+$ and CD34$^-$CD33$^+$ cells but spared CD34$^+$CD33^{dim} cells (supplemental Fig 2A). Additionally, contrary to resting CD4$^+$ cells and CD19$^+$ cells, highly mitotic polyhydroxic acid–stimulated CD4$^+$ cells and CD19$^+$ EBV LCLs became sensitive to effector CTLs because of increased expression of *hTERT* mRNA, the latter being more salient (Figure 5B and supplemental Fig 2B). Taken together, our findings suggest that gene-modified hTERT-specific CTLs will

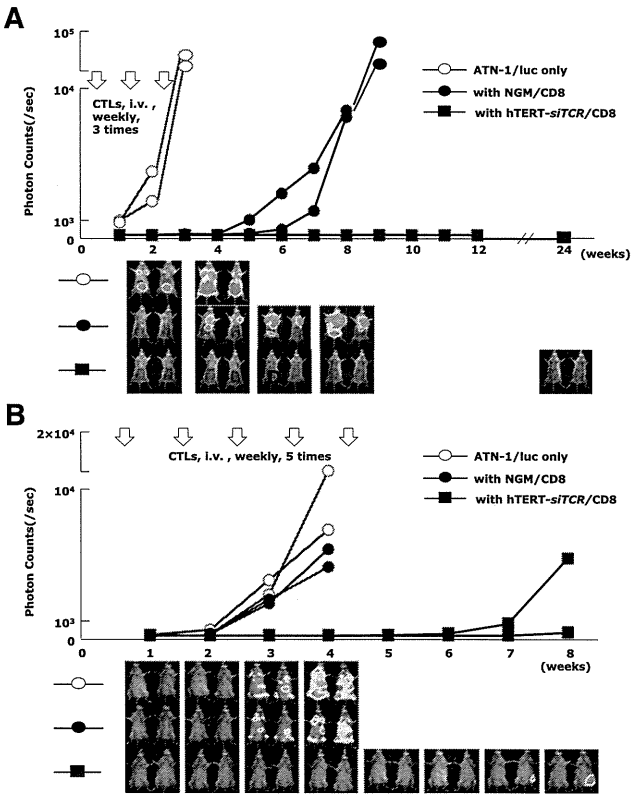

Figure 7. Anti-ATL reactivity of hTERT-*siTCR*–transduced CD8$^+$ T cells in vivo. (A) Winn assay. NOG mice were coinjected with a luciferase-transduced HLA-A*24:02$^+$ ATL cell line (ATN-1/luc) (5×10^5) and either 2.5×10^6 hTERT-*siTCR*–transduced (hTERT-*siTCR*/CD8) or NGM/CD8$^+$ T cells (n = 2 per group). Subsequently, 3 weekly infusions of the respective CD8$^+$ T-cell populations (2.5×10^6 cells per infusion) were administered intravenously (i.v.). Tumor growth was monitored every 7 days by using bioluminescence assay. Nontreated ATN-1/luc cells were similarly inoculated into NOG mice (n = 2) as a control. Although NGM/CD8 activated using OKT-3 and rhIL-2 suppressed tumor growth to some extent, hTERT-*siTCR*/CD8 durably suppressed tumor growth for longer than 6 months. (B) Therapeutic adaptive transfer model. NOG mice were intravenously inoculated with 5×10^5 ATN-1/luc cells. Four days later, intravenous administration of either 5×10^6 hTERT-*siTCR*/CD8 or NGM/CD8 (n = 2 per group) was started once a week for a total of 5 infusions. NOG mice given only ATN-1/luc cells (n = 2) were used as a control. In comparison with NGM/CD8, therapeutically infused hTERT-*siTCR*/CD8 also obviously suppressed the tumor cell growth within the 8-week observation period. Serial images of the bioluminescence assay demonstrate tumor growth in each group.

spare steady-state hematopoietic progenitor cells. However, to ensure safety, it would be better to avoid the active recovery phase of bone marrow after chemotherapy, notably under granulocyte colony-stimulating factor support, and also the acute infectious period in which immune-cell components are stimulated.

Another likely problem in clinical practice is that heavily pretreated peripheral lymphocytes from ATL patients might fail to proliferate. Proliferative activity of therapeutically infused gene-modified T cells in vivo is an important prerequisite for a successful outcome.[41] In this connection, although the control of treatment-related graft-versus-host disease still remains unsolved, use of CB lymphocytes has been investigated.[42] In this study, gene-modified CB-CD8$^+$ T cells from 2 donors successfully killed ATL tumor cells but spared autologous steady-state CB-CD34$^+$ cells (supplemental Figure 1-(2)). Compelling lack of suitable allo-HSCT donors for patients of advance age with ATL will encourage the application of CB transplantation using reduced-intensity preconditioning in the near future. Genetic redirection of CB lymphocytes using tumor antigen–specific *TCR* gene transfer will also play a considerable role.

Conversely, because hTERT is overexpressed in various kinds of cancer,[10] this approach may have widespread potential clinical application. Furthermore, the clinical availability of a new defucosylated anti-CCR4 mAb for treatment of ATL[43] can be reasonably anticipated to diminish regulatory T cells, the key player in the immunosuppressive microenvironment in patients with cancer,[44] because CCR4 is also expressed on regulatory T cells.[45] Therefore, hTERT-targeting immunotherapy after preconditioning with this anti-CCR4 mAb may become a realistically promising treatment option not only for ATL, but also for other malignancies.

In summary, using a newly established hTERT-*siTCR* vector, we have demonstrated the feasibility of anti-ATL redirected T-cell–based adoptive immunotherapy targeting hTERT, notably for patients who are ineligible for allo-HSCT. Further studies will be needed to investigate the clinical safety and utility of this novel therapy.

Acknowledgments

The authors are grateful for the skilled technical assistance of Dr Kenji Kameda, Ehime University, and Dr Hirofumi Inoue, Department of Biochemistry and Molecular Genetics, Ehime University Graduate School of Medicine. Thanks are also extended to Dr Yoshiki Akatsuka, Department of Hematology, Fujita Health University, for supplying the K562-A*24:02 cell line, Dr Midori Okumura and Dr Tomihiro Katayama, Department of Obstetrics and Gynecology, Ehime University Graduate School of Medicine, for supplying cord blood samples, and Dr Hiroo Saji, HLA Laboratory, Japan, for HLA typing.

This work was supported in part by grants from the Ministry of Education, Culture, Sports, Science and Technology of Japan (H.F., T.A., and M.Y.), a Grant-in-Aid for Cancer Research from the Ministry of Health, Labor and Welfare (M.Y.), and a grant from the Japan Leukemia Research Fund (2011) (H.F.).

Authorship

Contribution: Y.M. performed the research and wrote the paper; H.F. designed and performed the research, wrote and edited the paper and provided financial support; H.A., F.O., and T.O. performed the research and discussed the experimental results; T.A. interpreted the experimental results and provided financial support; T.I., S.O., J.M., K.K., and H.S. provided materials and discussed the experimental results; and M.Y. discussed and interpreted the experimental results and provided financial support.

Conflict-of-interest disclosure: The authors declare no competing financial interests.

Correspondence: Hiroshi Fujiwara, Department of Bioregulatory Medicine, Ehime University Graduate School of Medicine, Toon, Ehime 791-0295, Japan; e-mail: yunarief@m.ehime-u.ac.jp.

References

1. Uchiyama T, Yodoi J, Sagawa K, Takatsuki K, Uchino H. Adult T-cell leukemia: clinical and hematologic features of 16 cases. *Blood.* 1977; 50(3):481-492.
2. Matsuoka M, Jeang KT. Human T-cell leukaemia virus type 1 (HTLV-1) infectivity and cellular transformation. *Nat Rev Cancer.* 2007;7(4): 270-280.
3. Tsukasaki K, Utsunomiya A, Fukuda H, et al; Japan Clinical Oncology Group Study JCOG9801. VCAP-AMP-VECP compared with biweekly CHOP for adult T-cell leukemia-lymphoma: Japan Clinical Oncology Group Study JCOG9801. *J Clin Oncol.* 2007;25(34):5458-5464.
4. Hishizawa M, Kanda J, Utsunomiya A, et al. Transplantation of allogeneic hematopoietic stem cells for adult T-cell leukemia: a nationwide retrospective study. *Blood.* 2010;116(8): 1369-1376.
5. Kanda J, Hishizawa M, Utsunomiya A, et al. Impact of graft-versus-host disease on outcomes after allogeneic hematopoietic cell transplantation for adult T-cell leukemia: a retrospective cohort study. *Blood.* 2012;119(9):2141-2148.
6. Louis CU, Straathof K, Bollard CM, et al. Adoptive transfer of EBV-specific T cells results in sustained clinical responses in patients with locoregional nasopharyngeal carcinoma. *J Immunother.* 2010;33(9):983-990.
7. Kannagi M. Immunologic control of human T-cell leukemia virus type I and adult T-cell leukemia. *Int J Hematol.* 2007;86(2):113-117.
8. Suemori K, Fujiwara H, Ochi T, et al. HBZ is an immunogenic protein, but not a target antigen for human T-cell leukemia virus type 1-specific cytotoxic T lymphocytes. *J Gen Virol.* 2009; 90(Pt 8):1806-1811.
9. Nishikawa H, Maeda Y, Ishida T, et al. Cancer/testis antigens are novel targets of immunotherapy for adult T-cell leukemia/ lymphoma. *Blood.* 2012;119(13):3097-3104.
10. Patel KP, Vonderheide RH. Telomerase as a tumor-associated antigen for cancer immunotherapy. *Cytotechnology.* 2004;45(1-2): 91-99.
11. Sinha-Datta U, Horikawa I, Michishita E, et al. Transcriptional activation of hTERT through the NF-kappaB pathway in HTLV-I-transformed cells. *Blood.* 2004;104(8):2523-2531.
12. Hara T, Matsumura-Arioka Y, Ohtani K, Nakamura M. Role of human T-cell leukemia virus type I Tax in expression of the human telomerase reverse transcriptase (hTERT) gene in human T-cells. *Cancer Sci.* 2008;99(6):1155-1163.
13. Bellon M, Nicot C. Central role of PI3K in transcriptional activation of hTERT in HTLV-I-infected cells. *Blood.* 2008;112(7):2946-2955.
14. Brunsvig PF, Aamdal S, Gjertsen MK, et al. Telomerase peptide vaccination: a phase I/II study in patients with non-small cell lung cancer. *Cancer Immunol Immunother.* 2006;55(12): 1553-1564.
15. Domchek SM, Recio A, Mick R, et al. Telomerase-specific T-cell immunity in breast cancer: effect of vaccination on tumor immunosurveillance. *Cancer Res.* 2007;67(21):10546-10555.
16. Suso EM, Dueland S, Rasmussen AM, Vetrhus T, Aamdal S, Kvalheim G, Gaudernack G. hTERT mRNA dendritic cell vaccination: complete response in a pancreatic cancer patient associated with response against several hTERT epitopes. *Cancer Immunol Immunother.* 2011; 60(6):809-818.
17. Rapoport AP, Aqui NA, Stadtmauer EA, et al. Combination immunotherapy using adoptive T-cell transfer and tumor antigen vaccination on the basis of hTERT and survivin after ASCT for myeloma. *Blood.* 2011;117(3):788-797.
18. Arai J, Yasukawa M, Ohminami H, Kakimoto M, Hasegawa A, Fujita S. Identification of human telomerase reverse transcriptase-derived peptides that induce HLA-A24-restricted antileukemia cytotoxic T lymphocytes. *Blood.* 2001;97(9):2903-2907.
19. Tajima K, Ito Y, Demachi A, et al. Interferon-γ differentially regulates susceptibility of lung cancer cells to telomerase-specific cytotoxic

T lymphocytes. *Int J Cancer.* 2004;110(3):403-412.

20. Yasukawa M, Ochi T, Fujiwara H. Relapse of renal cell carcinoma with disappearance of HLA class I following hTERT peptide vaccination. *Ann Oncol.* 2010;21(10):2122-2124.
21. Yano H, Ishida T, Inagaki A, et al. Regulatory T-cell function of adult T-cell leukemia/lymphoma cells. *Int J Cancer.* 2007;120(9):2052-2057.
22. Johnson LA, Morgan RA, Dudley ME, et al. Gene therapy with human and mouse T-cell receptors mediates cancer regression and targets normal tissues expressing cognate antigen. *Blood.* 2009; 114(3):535-546.
23. Robbins PF, Morgan RA, Feldman SA, et al. Tumor regression in patients with metastatic synovial cell sarcoma and melanoma using genetically engineered lymphocytes reactive with NY-ESO-1. *J Clin Oncol.* 2011;29(7):917-924.
24. Pule MA, Savoldo B, Myers GD, et al. Virus-specific T cells engineered to coexpress tumor-specific receptors: persistence and antitumor activity in individuals with neuroblastoma. *Nat Med.* 2008;14(11):1264-1270.
25. Kalos M, Levine BL, Porter DL, Katz S, Grupp SA, Bagg A, June CH. T cells with chimeric antigen receptors have potent antitumor effects and can establish memory in patients with advanced leukemia. *Sci Transl Med.* 2011;3(95):95ra73.
26. Okamoto S, Mineno J, Ikeda H, Fujiwara H, Yasukawa M, Shiku H, Kato I. Improved expression and reactivity of transduced tumor-specific TCRs in human lymphocytes by specific silencing of endogenous TCR. *Cancer Res.* 2009; 69(23):9003-9011.
27. Okamoto S, Amaishi Y, Goto Y, et al. A promising vector for TCR gene therapy: Differential effect of siRNA, 2A peptide, and disulfide bond on the introduced TCR expression. *Mol Ther Nucleic Acids.* 2012;1:e63.
28. Naoe T, Akao Y, Yamada K, et al. Cytogenetic characterization of a T-cell line, ATN-1, derived from adult T-cell leukemia cells. *Cancer Genet Cytogenet.* 1988;34(1):77-88.
29. Fukudome K, Furuse M, Fukuhara N, et al. Strong induction of ICAM-1 in human T cells transformed by human T-cell-leukemia virus type 1 and depression of ICAM-1 or LFA-1 in adult T-cell-leukemia-derived cell lines. *Int J Cancer.* 1992; 52(3):418-427.
30. Sugamura K, Fujii M, Kannagi M, Sakitani M, Takeuchi M, Hinuma Y. Cell surface phenotypes and expression of viral antigens of various human cell lines carrying human T-cell leukemia virus. *Int J Cancer.* 1984;34(2):221-228.
31. Sugamura K, Nakai S, Fujii M, Hinuma Y. Interleukin 2 inhibits in vitro growth of human T cell lines carrying retrovirus. *J Exp Med.* 1985; 161(5):1243-1248.
32. Miyoshi I, Kubonishi I, Yoshimoto S, et al. Type C virus particles in a cord T-cell line derived by co-cultivating normal human cord leukocytes and human leukaemic T cells. *Nature.* 1981; 294(5843):770-771.
33. Harada S, Koyanagi Y, Yamamoto N. Infection of HTLV-III/LAV in HTLV-I-carrying cells MT-2 and MT-4 and application in a plaque assay. *Science.* 1985;229(4713):563-566.
34. Ochi T, Fujiwara H, Okamoto S, et al. Novel adoptive T-cell immunotherapy using a WT1-specific TCR vector encoding silencers for endogenous TCRs shows marked antileukemia reactivity and safety. *Blood.* 2011;118(6): 1495-1503.
35. Ochi T, Fujiwara H, Suemori K, et al. Aurora-A kinase: a novel target of cellular immunotherapy for leukemia. *Blood.* 2009;113(1):66-74.
36. Nagai K, Ochi T, Fujiwara H, et al. Aurora kinase A-specific T-cell receptor gene transfer redirects T lymphocytes to display effective antileukemia reactivity. *Blood.* 2012;119(2): 368-376.
37. Ito M, Hiramatsu H, Kobayashi K, et al. NOD/SCID/gamma(c)(null) mouse: an excellent recipient mouse model for engraftment of human cells. *Blood.* 2002;100(9):3175-3182.
38. Kuhlmann AS, Villaudy J, Gazzolo L, Castellazzi M, Mesnard JM, Duc Dodon M. HTLV-1 HBZ cooperates with JunD to enhance transcription of the human telomerase reverse transcriptase gene (hTERT). *Retrovirology.* 2007;4:92.
39. Bendle GM, Linnemann C, Hooijkaas AI, et al. Lethal graft-versus-host disease in mouse models of T cell receptor gene therapy. *Nat Med.* 2010; 16(5):565-570, 1p, 570.
40. Dolcetti R, De Rossi A. Telomere/telomerase interplay in virus-driven and virus-independent lymphomagenesis: pathogenic and clinical implications. *Med Res Rev.* 2012;32(2): 233-253.
41. Ochi T, Fujiwara H, Yasukawa M. Requisite considerations for successful adoptive immunotherapy with engineered T-lymphocytes using tumor antigen-specific T-cell receptor gene transfer. *Expert Opin Biol Ther.* 2011;11(6): 699-713.
42. Frumento G, Zheng Y, Aubert G, et al. Cord blood T cells retain early differentiation phenotype suitable for immunotherapy after TCR gene transfer to confer EBV specificity. *Am J Transplant.* 2013;13(1):45-55.
43. Ishida T, Joh T, Uike N, et al. Defucosylated anti-CCR4 monoclonal antibody (KW-0761) for relapsed adult T-cell leukemia-lymphoma: a multicenter phase II study. *J Clin Oncol.* 2012; 30(8):837-842.
44. Byrne WL, Mills KH, Lederer JA, O'Sullivan GC. Targeting regulatory T cells in cancer. *Cancer Res.* 2011;71(22):6915-6920.
45. Iellem A, Mariani M, Lang R, Recalde H, Panina-Bordignon P, Sinigaglia F, D'Ambrosio D. Unique chemotactic response profile and specific expression of chemokine receptors CCR4 and CCR8 by CD4(+)CD25(+) regulatory T cells. *J Exp Med.* 2001;194(6):847-853.

Vaccine 31 (2013) 2110–2118

Contents lists available at SciVerse ScienceDirect

Vaccine

journal homepage: www.elsevier.com/locate/vaccine

Establishment of animal models to analyze the kinetics and distribution of human tumor antigen-specific CD8$^+$ T cells

Daisuke Muraoka[a,d], Hiroyoshi Nishikawa[a,e,*], Takuro Noguchi[a,f], Linan Wang[b], Naozumi Harada[a,d], Eiichi Sato[g], Immanuel Luescher[h], Eiichi Nakayama[i], Takuma Kato[c], Hiroshi Shiku[a,b,1]

[a] Departments of Cancer Vaccine, Mie University Graduate School of Medicine, Mie 514-8507, Japan
[b] Departments of Immuno-Gene Therapy, Mie University Graduate School of Medicine, Mie 514-8507, Japan
[c] Departments of Cellular and Molecular Immunology, Mie University Graduate School of Medicine, Mie 514-8507, Japan
[d] Immunofrontier, Inc., Tokyo, 143-0023, Japan
[e] Experimental Immunology, Immunology Frontier Research Center, Osaka University, Osaka, 565-0871, Japan
[f] Ludwig Institute for Cancer Research, New York Branch, Memorial Sloan-Kettering Cancer Center, New York, NY 10065, United States
[g] Department of Anatomic Pathology, Tokyo Medical University, Tokyo, 160-8402, Japan
[h] Ludwig Institute for Cancer Research, Lausanne Branch, University of Lausanne, Epalinges, 1066, Switzerland
[i] Faculty of Health and Welfare, Kawasaki University of Medical Welfare, Okayama, 701-0193, Japan

ARTICLE INFO

Article history:
Received 21 January 2013
Accepted 27 February 2013
Available online 13 March 2013

Keywords:
Translational research
Animal model
Cancer vaccine
Immune responses
CD8$^+$ T cells
Cacer/testis antigens

ABSTRACT

Many patients develop tumor antigen-specific T cell responses detectable in peripheral blood mononuclear cells (PBMCs) following cancer vaccine. However, measurable tumor regression is observed in a limited number of patients receiving cancer vaccines. There is a need to re-evaluate systemically the immune responses induced by cancer vaccines. Here, we established animal models targeting two human cancer/testis antigens, NY-ESO-1 and MAGE-A4. Cytotoxic T lymphocyte (CTL) epitopes of these antigens were investigated by immunizing BALB/c mice with plasmids encoding the entire sequences of NY-ESO-1 or MAGE-A4. CD8$^+$ T cells specific for NY-ESO-1 or MAGE-A4 were able to be detected by ELISPOT assays using antigen presenting cells pulsed with overlapping peptides covering the whole protein, indicating the high immunogenicity of these antigens in mice. Truncation of these peptides revealed that NY-ESO-1-specific CD8$^+$ T cells recognized D^d-restricted 8mer peptides, NY-ESO-1$_{81\text{-}88}$. MAGE-A4-specific CD8$^+$ T cells recognized D^d-restricted 9mer peptides, MAGE-A4$_{265\text{-}273}$. MHC/peptide tetramers allowed us to analyze the kinetics and distribution of the antigen-specific immune responses, and we found that stronger antigen-specific CD8$^+$ T cell responses were required for more effective anti-tumor activity. Taken together, these animal models are valuable for evaluation of immune responses and optimization of the efficacy of cancer vaccines.

1. Introduction

A number of cancer vaccine strategies targeting tumor antigens recognized by the human immune system have been tested [1–3]. While many of these cancer vaccines elicited measurable immune responses detectable in peripheral blood mononuclear cells (PBMCs), only a subset of treated patients experienced clinical benefits, such as tumor regression [4,5]. Because of the weak clinical effectiveness of currently available cancer vaccines, not only new immunogenic antigens, effective adjuvant formulations, vectors or vaccination methods but also new methodologies to evaluate efficacy of cancer vaccines are required.

NY-ESO-1, a germ line cell protein detected by SEREX (serological identification of antigens by recombinant expression cloning) using the serum of an esophageal cancer patient, is often expressed by cancer cells, but not by normal somatic cells [3,6]. This ideal expression pattern facilitated the study of this antigen; including immuno-monitoring of cancer patients with NY-ESO-1-expressing tumors and clinical trials that focused on NY-ESO-1 [3]. While these studies have revealed that a number of different cancer vaccines, including short and overlapping peptides, protein, viral vectors and DNA, resulted in development of measurable immune responses,

Abbreviations: APC, antigen presenting cells; CTL, cytotoxic T lymphocyte; dLN, draining lymph node; ELISPOT assay, enzyme-linked immunospot assay; IFN, interferon; mAb, monoclonal antibody; PBMC, peripheral blood mononuclear cells.

* Corresponding author at: Experimental Immunology, Immunology Frontier Research Center, Osaka University, 3-1 Yamadaoka, Suita, Osaka 565-0871, Japan. Tel.: +81 6 6879 4963; fax: +81 6 6879 4464.
E-mail addresses: nisihiro@ifrec.osaka-u.ac.jp (H. Nishikawa), shiku@clin.medic.mie-u.ac.jp (H. Shiku).
[1] Departments of Cancer Vaccine and Immuno-Gene Therapy, Mie University Graduate School of Medicine, 2-174 Edobashi, Tsu, Mie 514-8507, Japan. Tel.: +81 59 231 5062; fax: +81 59 231 5276.

0264-410X/$ – see front matter © 2013 Elsevier Ltd. All rights reserved.
http://dx.doi.org/10.1016/j.vaccine.2013.02.056

correlations between immunological and clinical responses were often week or difficult to observe [3].

MAGE-A4, another cancer/testis (CT) antigen, elicits MAGE-A4-specific $CD4^+$ and $CD8^+$ T cell responses in some patients with MAGE-A4-expressing cancers, indicating that MAGE-A4 is also an immunogenic protein [7–9]. We have recently reported a novel MAGE-A4 epitope presented by human leukocyte antigen (HLA)-A*2402 using a $CD8^+$ T cell clone 2-28 [9]. As this clone effectively killed tumor cell lines that expressed both MAGE-A4 and HLA-A*2402, this antigen could be a candidate for a cancer vaccine.

Given the poor correlation between the immune responses detected in PBMCs and clinical responses [2,3,5], it is necessary to re-evaluate existing cancer immunotherapy strategies in detail using animal models, namely reverse translational research. To this end, we developed animal models involving human tumor antigens, such as NY-ESO-1 or MAGE-A4 in this study.

2. Materials and methods

2.1. Mice

Female BALB/c mice were purchased from SLC Japan (Shizuoka, Japan) and used at 7–10 weeks of age. They were maintained at the Animal Center of Mie University Graduate School of Medicine (Mie, Japan). The experimental protocol was approved by the Ethics Review Committee for Animal Experimentation of Mie University Graduate School of Medicine.

2.2. Antibodies and reagents

Anti-H2-K^d (KD40, mouse IgG2a), anti-H2-D^d (DD98, mouse IgG2a), and anti-H2-L^d (30-5-7, mouse IgG2a) were produced and purified from each hybridoma. FITC-conjugated anti-CD8 mAb (53-6.7, rat IgG2a) and APC-conjugated anti-CD4 mAb (GK1.5, rat IgG2b) were purchased from BD Biosciences (Franklin Lakes, NJ). PE-conjugated anti-Foxp3 mAb (Fjk16s, rat IgG2a) was purchased from eBiosciences (San Diego, CA). Synthetic NY-ESO-1 and MAGE-A4 peptides (summarized in Supplementary Table 1) were obtained from Sigma Genosys (Hokkaido, Japan).

2.3. Immunization using a gene gun

Naive BALB/c mice were immunized twice at two-week intervals. Gold particles coated with 1 μg of each plasmid DNA were prepared and delivered into the shaved skin of the abdominal wall of BALB/c mice using a Helios Gene Gun System (BioRad, Hercules, CA) at a helium discharge pressure of 350–400 psi, as described previously [10,11].

2.4. Cell isolation

Spleen cell suspensions were mixed with CD8 Microbeads (Miltenyi Biotec, Bergisch Gladbach, Germany) and separated into $CD8^+$ T cells by positive selection on a MACS column. The isolated $CD8^+$ T cell populations were confirmed to contain >95% $CD8^+$ T cells.

2.5. Enzyme-linked immunospot (ELISPOT) assay

The number of IFN-γ secreting antigen-specific $CD8^+$ T cells was assessed by ELISPOT assay as described previously [10,11]. Briefly, purified $CD8^+$ T cells were cultured for 24 hours with 5×10^5 irradiated CD90-depleted splenocytes pulsed with the indicated peptides in 96-well nitrocellulose-coated microtiter plates (Millipore, Bedford, MA) coated with rat anti-mouse IFN-γ mAb (R4-6A2, BD Biosciences). Spots were developed using biotinylated anti-mouse IFN-γmAb (XMG1.2, BD Biosciences), alkaline phosphatase conjugated streptavidin (MABTECH, Sweden) and alkaline phosphatase substrate kit (BioRad), and subsequently counted.

2.6. ELISA

96-well flat-bottomed microliter plates (Immuno-NUNC) were coated with 20 ng/50 μml of NY-ESO-1 or MAGE-A4 protein, respectively, at 4 °C overnight. Wells were blocked with 1% BSA/PBS for 1 hour at room temperature and washed three times. Serum (1:100 dilution) was added and incubated at 4 °C overnight. After washing, goat anti-mouse IgG antibody conjugated with horseradish peroxidase (Promega, Madison, WI) was added (1:5000 dilution). Two hours later, color was developed with TMB substrate solution (Thermo scientific, IL) and stopped with H_2SO_4. The absorbance was measured at 450 nm and calculated after subtraction of the absorbance value of control wells without sera.

2.7. Flow cytometry and tetramer staining

Tetramer staining was performed as described previously [11]. Briefly, cells were stained with PE-labeled NY-ESO-$1_{81-88}/D^d$ or MAGE-$A4_{265-273}/D^d$ tetramers (prepared at the Ludwig Institute Core Facility, Lausanne, Switzerland) for 10 minutes at 37 °C before additional staining of surface markers for 15 minutes at 4 °C. After washing, the results were analyzed on FACSCanto (BD Biosciences) and FlowJo software (Tree Star, Ashland, OR).

2.8. Tumors

CT26 is a colon epithelial tumor derived by intrarectal injections of N-nitroso-N-methylurethane in BALB/c mice [12]. CT26 expressing NY-ESO-1 or MAGE-A4, a human cancer/testis antigen were established as described previously [11,13].

2.9. Statistical analysis

Values were expressed as mean ± SD. Differences between groups were examined for statistical significance using the Student's *t*-test. *p* values <0.05 were considered statistically significant.

3. Results

3.1. NY-ESO-1-specific $CD8^+$ T cells recognize D^d-restricted NY-ESO-1_{81-88} peptide

We analyzed the minimal epitope recognized by NY-ESO-1-specific $CD8^+$ T cells after immunization with NY-ESO-1. To this end, we employed a Helios Gene Gun System as we have previously detected NY-ESO-1-specific $CD8^+$ T cell responses [10,11]. To identify minimal epitopes, naive BALB/c mice were immunized twice at two-week intervals with plasmids encoding the entire sequence of NY-ESO-1. $CD8^+$ T cells were obtained from spleens and specific T cell responses were analyzed by ELISPOT assay using peptide pools shown in Supplementary Table 1. A significant number of NY-ESO-1-specific $CD8^+$ T cells was detected against peptide pool #3 (Fig. 1A). To identify the NY-ESO-1 epitope, NY-ESO-1-specific $CD8^+$ T cells were stimulated with each of these peptides. IFN-γ secretion was observed when NY-ESO-1-specific $CD8^+$ T cells were stimulated with 71–90 and 81–100 NY-ESO-1 peptides, suggesting the presence of a minimal epitope within 81–90 residues (Fig. 1B). To determine the minimal epitope, the 81–90 peptide of NY-ESO-1 was further truncated. NY-ESO-1-specific $CD8^+$ T cells recognized the 80–88 and 81–88, but not 80–87 or 82–88 peptides, thus

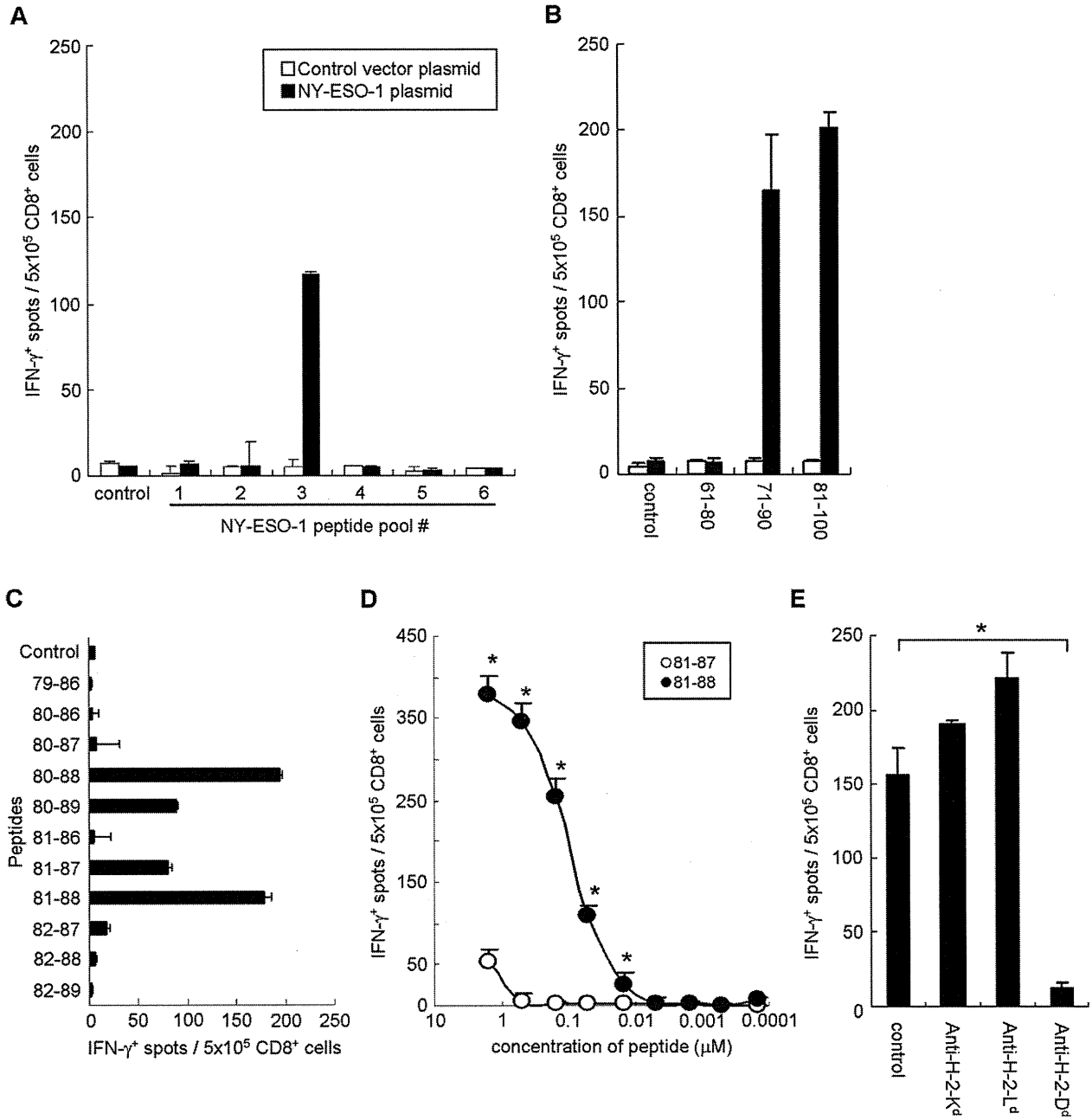

Fig. 1. NY-ESO-1-specific CD8$^+$ T cells recognize D^d-restricted NY-ESO-1$_{81-88}$ peptide. (A–C) BALB/c mice were immunized by gene gun twice at two-week intervals with plasmids encoding the entire sequence of NY-ESO-1. CD8$^+$ T cells were obtained from spleens and specific T cells were analyzed with ELISPOT assay using APCs pulsed with the indicated peptides. (D) Avidity of induced NY-ESO-1-specific CD8$^+$ T cells was analyzed with ELISPOT assay using APCs pulsed with graded doses of peptides ranging from 3 to 0.0001 μM. (E) MHC restriction of induced NY-ESO-1-specific CD8$^+$ T cells was analyzed with ELISPOT assay by the addition of anti-H-2-K^d, anti-H-2-D^d or anti-H-2-L^d mAbs. These experiments were repeated two to four times with similar results. Data are mean ± SD.

the minimal epitope was identified to be NY-ESO-1$_{81-88}$ peptide (Fig. 1C).

To confirm this, graded doses of the peptides were pulsed on antigen presenting cells (APCs) and specific IFN-γ secretion was analyzed by ELISPOT assay. NY-ESO-1-specific CD8$^+$ T cells were high-avidity, and capable to recognize as little as 30 nM of peptide (Fig. 1D), confirming that NY-ESO-1$_{81-88}$ peptide is the minimal epitope. Next, we assessed the restriction of this response using blocking antibodies. NY-ESO-1-specific CD8$^+$ T cell responses were completely blocked by addition of anti-H-2-D^d mAb (Fig. 1E). Taken together, NY-ESO-1-specific CD8$^+$ T cells recognize D^d-restricted NY-ESO-1$_{81-88}$ peptide.

3.2. MAGE-A4-specific CD8$^+$ T cells recognize D^d-restricted MAGE-A4$_{265-273}$ peptide

To establish a MAGE-A4 animal model, we determined the minimal epitope of MAGE-A4-specific CD8$^+$ T cells after immunization with MAGE-A4. Naive BALB/c mice were immunized twice at two-week intervals with plasmids encoding the entire sequence of MAGE-A4. Splenic CD8$^+$ T cells were prepared and specific T cell responses were analyzed by ELISPOT assay using peptide pools shown in Supplementary Table 1. MAGE-A4-specific CD8$^+$ T cells were induced in mice immunized with plasmids encoding MAGE-A4 within peptide pool #5 (Fig. 2A). To elucidate the dominant

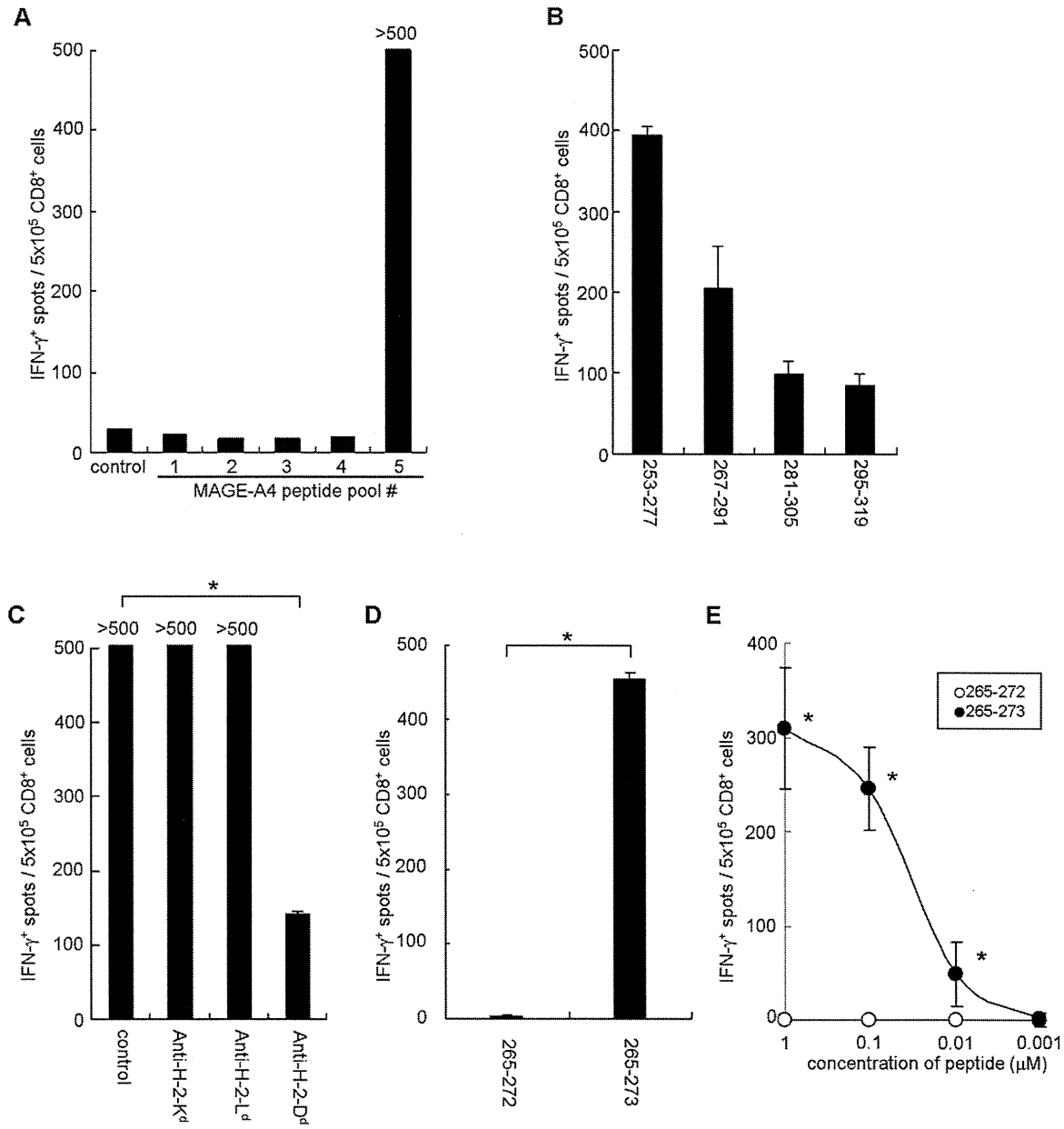

Fig. 2. MAGE-A4-specific CD8+ T cells recognize D^d-restricted MAGE-$A4_{265-273}$ peptide. (A, B) BALB/c mice were immunized by gene gun twice at two-week intervals with plasmids encoding the entire sequence of MAGE-A4. CD8+ T cells were obtained from spleens, and specific T cells were analyzed with ELISPOT assay using APCs pulsed with the indicated peptides. (C) MHC restriction of induced MAGE-A4-specific CD8+ T cells was analyzed with ELISPOT assay by the addition of the indicated mAb. (D) MAGE-$A4_{253-277}$ was subjected to BIMAS program and the highest score within MAGE-$A4_{253-277}$ for a D^d binding motif was predicted in 265–272 and 265–273 of MAGE-A4. These predicted peptides were analyzed with ELISPOT assay for identification of MAGE-A4 epitope peptide. (E) Avidity of MAGE-A4-specific CD8+ T cells was analyzed with ELISPOT assay using APCs pulsed with graded doses of peptides. These experiments were repeated two to four times with similar results. Data are mean ± SD.

MAGE-A4 epitope, MAGE-A4-specific CD8+ T cells were stimulated with each of the peptides from pool #5. The 253–277 peptide was most effective for stimulating MAGE-A4-specific CD8+ T cells (Fig. 2B). We next assessed the restriction of this response using blocking antibodies. MAGE-A4-specific CD8+ T cell responses were completely blocked by anti-H-2 D^d mAb (Fig. 2C). Given the H-2 D^d restriction of this CD8+ T cell response, we employed computer-based BIMAS program to predict optimized MHC class I epitope within the MAGE-$A4_{253-277}$ peptide. This program ranks all the possible MHC class I epitopes within a given polypeptide sequence. MAGE-$A4_{253-277}$ was subjected to this program and the highest score within MAGE-$A4_{253-277}$ for a D^d binding motif was predicted in 265–272 and 265–273 of MAGE-A4 (Supplementary Table 2). MAGE-A4-specific CD8+ T cells recognized the 265–273, but not 265–272 peptides, thus the minimal epitope was considered to be the MAGE-$A4_{265-273}$ peptide (Fig. 2D). To confirm this minimal epitope, graded doses of peptides were pulsed on APC and specific IFN-γ secretion was analyzed by ELISPOT assay. MAGE-A4-specific CD8+ T cells were high avidity, and could recognize as little as 10 nM of the peptide (Fig. 2E). We conclude that MAGE-A4-specific CD8+ T cells recognize D^d-restricted MAGE-$A4_{265-273}$ peptide.

3.3. *Kinetics and distribution of NY-ESO-1/MAGE-A4-specific CD8+ T cells after gene gun immunization*

Next, we generated MHC/peptide tetramers based on the data of minimal epitope and MHC restriction for NY-ESO-1/MAGE-A4-specific CD8+ T cells. BALB/c mice were immunized with plasmids

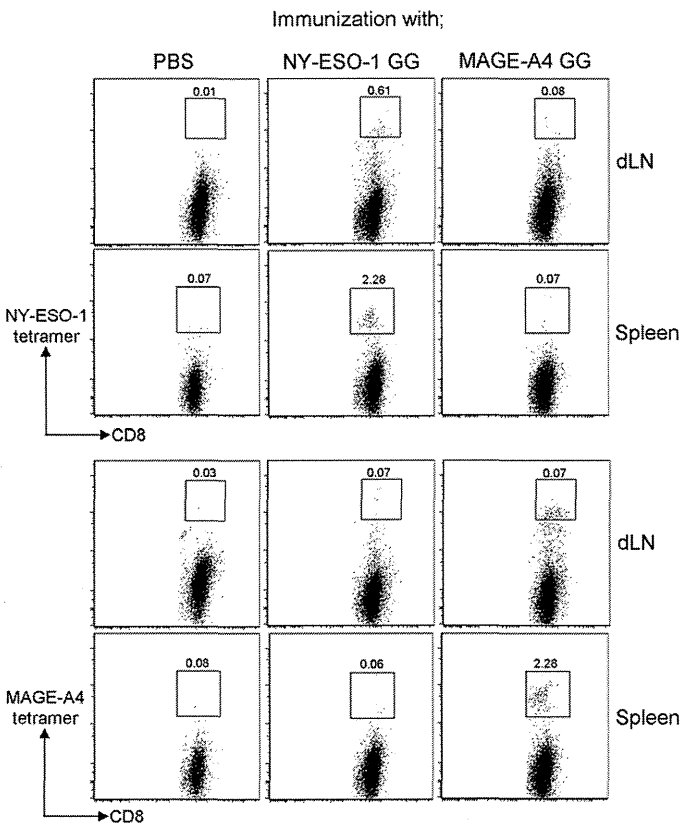

Fig. 3. NY-ESO-1/MAGE-A4-specific CD8$^+$ T cells are detected after immunization with a gene gun. BALB/c mice were immunized twice at two-week intervals with plasmids encoding the entire sequences of NY-ESO-1 or MAGE-A4 using a gene gun. Seven days after the second vaccination, CD8$^+$ T cells were obtained from the draining lymph nodes (dLNs) and spleens, and specific T cells were analyzed with MHC/peptide tetramer assay. These experiments were repeated two to four times with similar results. GG: gene gun.

encoding the whole sequences of NY-ESO-1 or MAGE-A4 by gene gun and the kinetics and distribution of NY-ESO-1/MAGE-A4-specific CD8$^+$ T cells were analyzed with MHC/peptide tetramers. NY-ESO-1-specific CD8$^+$ T cells were detected 7–10 days after the primary immunization both in draining lymph nodes and spleens in mice immunized with plasmids encoding NY-ESO-1, but not in mice immunized with MAGE-A4 or control mice (Fig. 3, 4A and 4B). NY-ESO-1-specific T cell responses were further enhanced by the secondary vaccination in both the draining lymph nodes and spleens (Fig. 4A and B). Similarly, MAGE-A4-specific CD8$^+$ T cells were detected 7–10 days after the primary immunization by gene gun in both the draining lymph nodes and spleens and were enhanced after the booster vaccination (Figs. 3, 4C and 4D), suggesting that these assays are useful tools for analyzing the kinetics and distribution of these antigen-specific CD8$^+$ T cells.

3.4. NY-ESO-1-specific CD8$^+$ T cell responses are primed spontaneously after tumor inoculation and these cells partially inhibit tumor growth

It is important to establish tumor models to re-evaluate cancer immunotherapy strategies in detail. To this end, we employed CT26 (a murine colon carcinoma) tumor transplantation model with stable expression of NY-ESO-1 and examined NY-ESO-1-specific CD8$^+$ T cell and humoral responses spontaneously primed in tumor bearing animals. BALB/c mice were inoculated with CT26-NY-ESO-1 and specific CD8$^+$ T cell and Ab responses were analyzed with MHC/peptide tetramers and ELISA, respectively. NY-ESO-1-specific CD8$^+$ T cells were spontaneously primed 7 days after tumor inoculation in the draining lymph nodes, spleens and peripheral blood in mice inoculated with CT26-NY-ESO-1 and augmented thereafter (Fig. 5A). We then addressed whether these spontaneously-primed NY-ESO-1-specific CD8$^+$ T cells were involved in tumor growth inhibition. To deplete these CD8$^+$ T cells, tumor bearing mice were injected with anti-CD8 mAb and tumor growth was analyzed. Anti-CD8 mAb administration augmented tumor growth compared with the control group without any treatment (Fig. 5C), suggesting an anti-tumor role of spontaneously-primed NY-ESO-1-specific CD8$^+$ T cells. On the other hand, NY-ESO-1-specific Ab responses were not observed 7 days after tumor inoculation, but detected 21 days after tumor inoculation (Fig. 5B). This is compatible with immunological monitoring in humans showing that higher stage of melanoma patients frequently develop humoral immune responses against NY-ESO-1 [3,14].

We next immunized these mice with plasmids encoding the entire sequence of NY-ESO-1 and anti-tumor activity was examined. Tumor growth was significantly reduced by immunization with NY-ESO-1 as compared to the control group without treatment (Fig. 5C). Furthermore, CD8$^+$ T cell depletion totally abolished the anti-tumor effects induced by DNA vaccine (Fig. 5C). As CD4$^+$ regulatory T cells (Tregs) are reportedly associated with spontaneously-primed and treatment-induced anti-tumor immune responses [15], we also investigated tumor-infiltrating Tregs. While Tregs were present in tumors, their frequency was not associated with anti-tumor activity induced by immunization with plasmids encoding NY-ESO-1 (Fig. 5D). Together, CD8$^+$ T cell and Ab responses to NY-ESO-1 in this tumor model closely parallel NY-ESO-1 immune responses in humans. Spontaneous tumor antigen-specific immune responses restrained, albeit incomplete, tumor growth, but tumor growth were vigorous and overwhelmed the tumor growth inhibition, thus additional augmentation of these immune responses are required for effective control of tumor growth.

3.5. MAGE-A4-specific CD8$^+$ T cell responses is primed spontaneously after tumor inoculation

We established another tumor transplantation model with stable expression of MAGE-A4 and examined MAGE-A4-specific CD8$^+$ T cell and humoral responses spontaneously primed in tumor bearing mice. BALB/c mice were inoculated with CT26-MAGE-A4 and specific CD8$^+$ T cell and humoral responses were analyzed with MHC/peptide tetramers and ELISA. In these mice, MAGE-A4-specific CD8$^+$ T cells were spontaneously primed 7 days after tumor inoculation in the draining lymph nodes, spleen and PBMC, and augmented thereafter (Fig. 6A). MAGE-A4-specific Ab responses were not observed 7 days after tumor inoculation, but detected 21 days after tumor inoculation (Fig. 6B). Like as the result of NY-ESO-1 models, cellular and humoral immune responses to MAGE-A4 in this model closely parallel MAGE-A4 immune responses in humans.

4. Discussion

We have established mouse models that allowed studies on NY-ESO-1 and MAGE-A4 immunity. Using these models, we evaluated the kinetics and distribution of antigen-specific CD8$^+$ T cells after tumor growth and immunization. While it has been recently shown that CD4$^+$CD25$^+$ Tregs and the ratio of CD8$^+$ effector T cells to Tregs in tumors critically influenced the prognosis of cancer patients [16,17], limitation of samples usually makes it difficult to investigate the function of effector T cells and Tregs at tumor sites in humans. Given the importance of tumors as active sites of anti-tumor responses, it is important to examine not only the draining

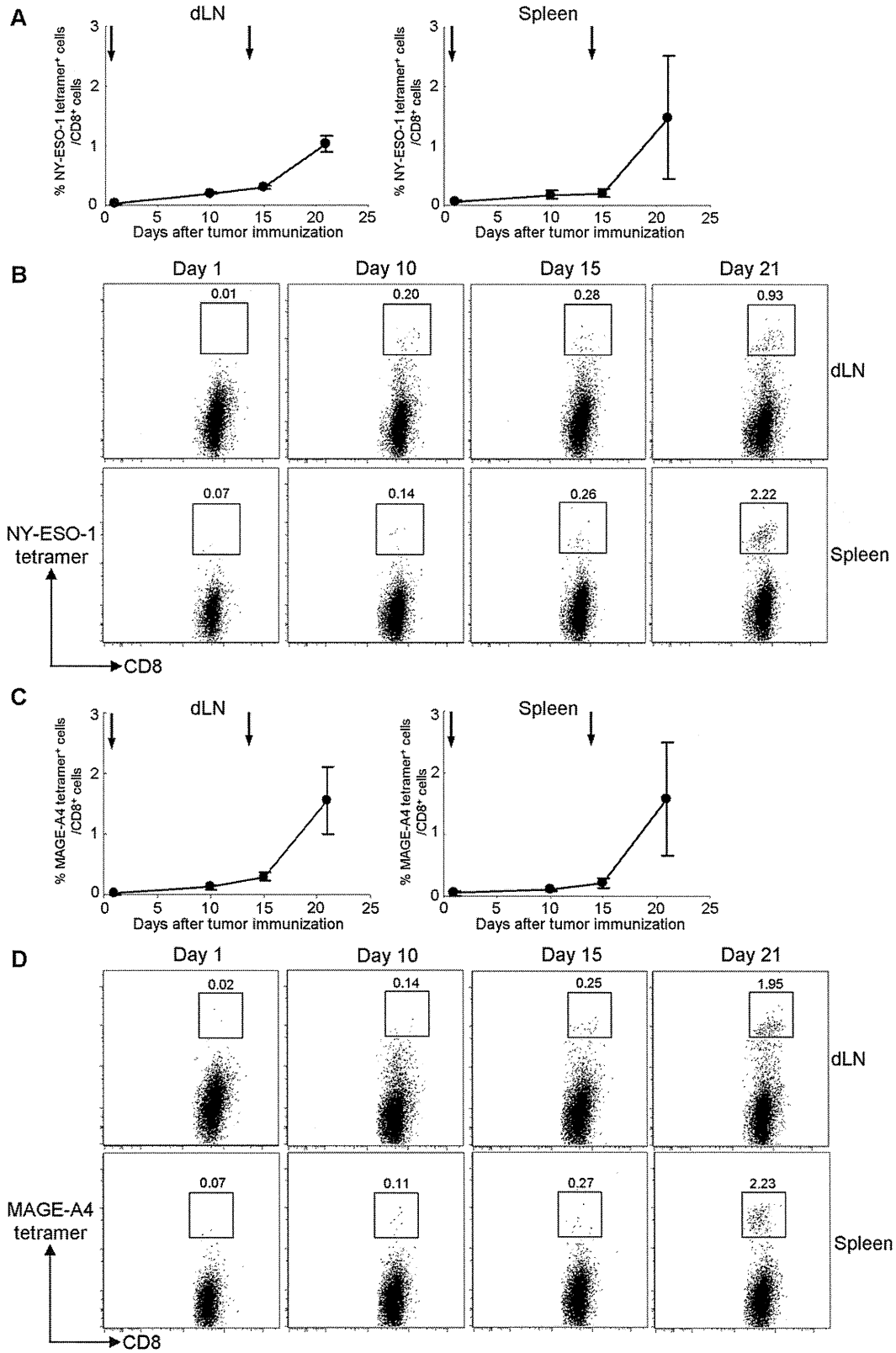

Fig. 4. Kinetics and distribution of NY-ESO-1/MAGE-A4-specific CD8+ T cells after immunization with a gene gun. Kinetics and distribution of NY-ESO-1 (A and B)/MAGE-A4 (C and D)-specific CD8+ T cells were analyzed by MHC/peptide tetramer assay. BALB/c mice were immunized twice at two-week intervals with plasmids encoding the entire sequence of either NY-ESO-1 or MAGE-A4 using a gene gun. CD8+ T cells were obtained from the draining lymph nodes (dLNs) and spleens on the indicated days, and specific T cells was analyzed with MHC/peptide tetramer assay. These experiments were repeated two to four times with similar results. Data in (A) and (C) are mean ± SD. Arrows in (A) and (C) represent the first and second immunization.

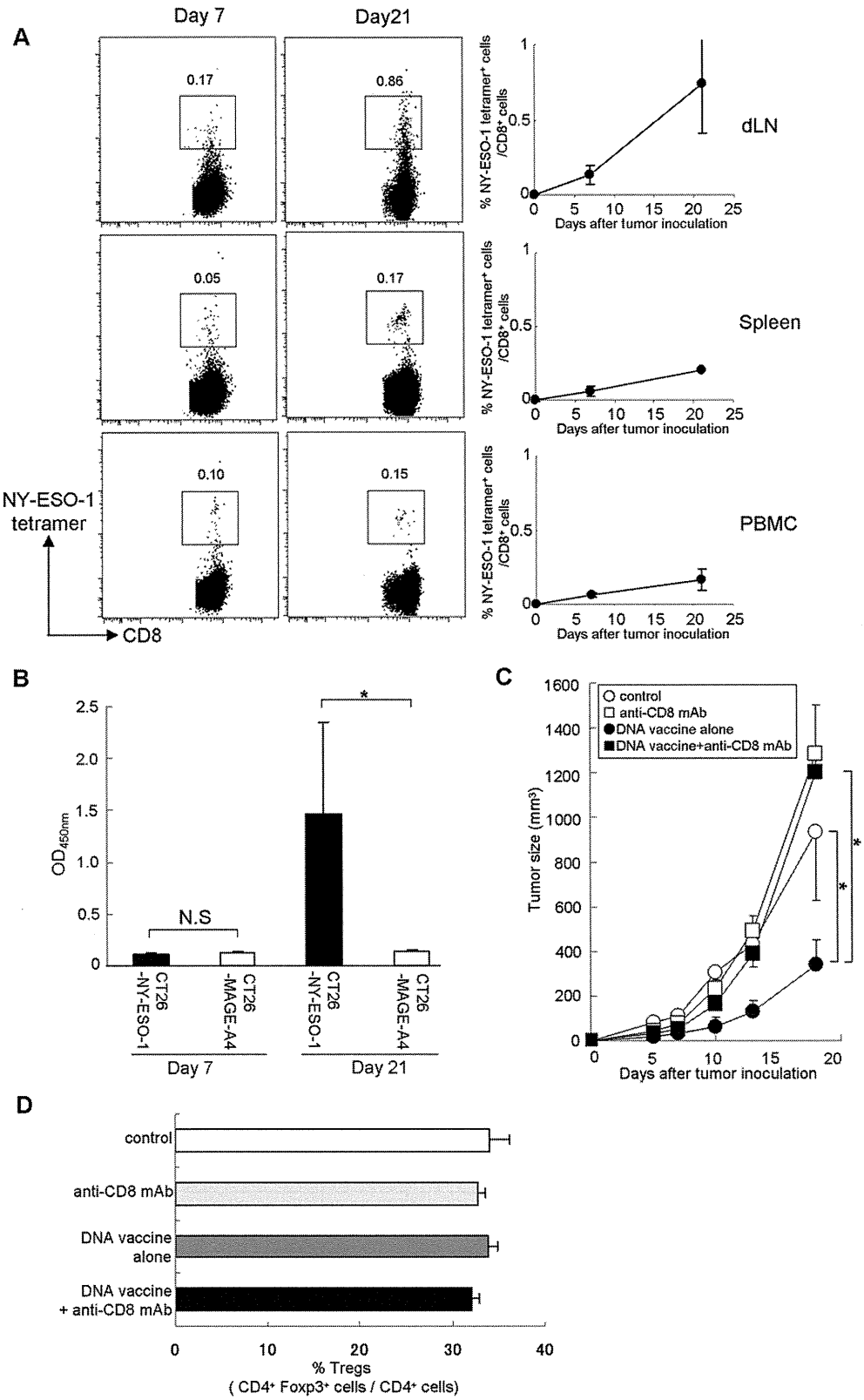

Fig. 5. NY-ESO-1-specific $CD8^+$ T cells are primed spontaneously after tumor inoculation, and these cells partially inhibit tumor growth. BALB/c mice were inoculated with CT26-NY-ESO-1. (A) $CD8^+$ T cells were isolated from the draining lymph nodes (dLNs), spleens and PBMCs on the indicated days, and NY-ESO-1-specific T cells were analyzed with MHC/peptide tetramer assay. (B) Sera were obtained on the indicated days and Ab responses against NY-ESO-1 were analyzed with ELISA. These experiments were repeated twice with similar results. Data are mean ± SD. $^*p < 0.05$ as compared to control. (C) BALB/c mice were immunized with plasmids encoding the entire sequence of NY-ESO-1, and CT26-NYESO-1 was inoculated on day 21 (one week after final immunization). Indicated groups of mice were administered with anti-CD8 mAb (clone 19/178, 100 μg/mouse, every 12 days). More than 95% of $CD8^+$ T cells were depleted by this method (data not shown). Each group consisted of four mice. Mice were monitored thrice a week. These experiments were repeated two times with similar results. (D) Tumor infiltrating lymphocytes were collected 21 days after tumor inoculation and the frequency of $Foxp3^+$ cells in $CD4^+$ T cells was analyzed.

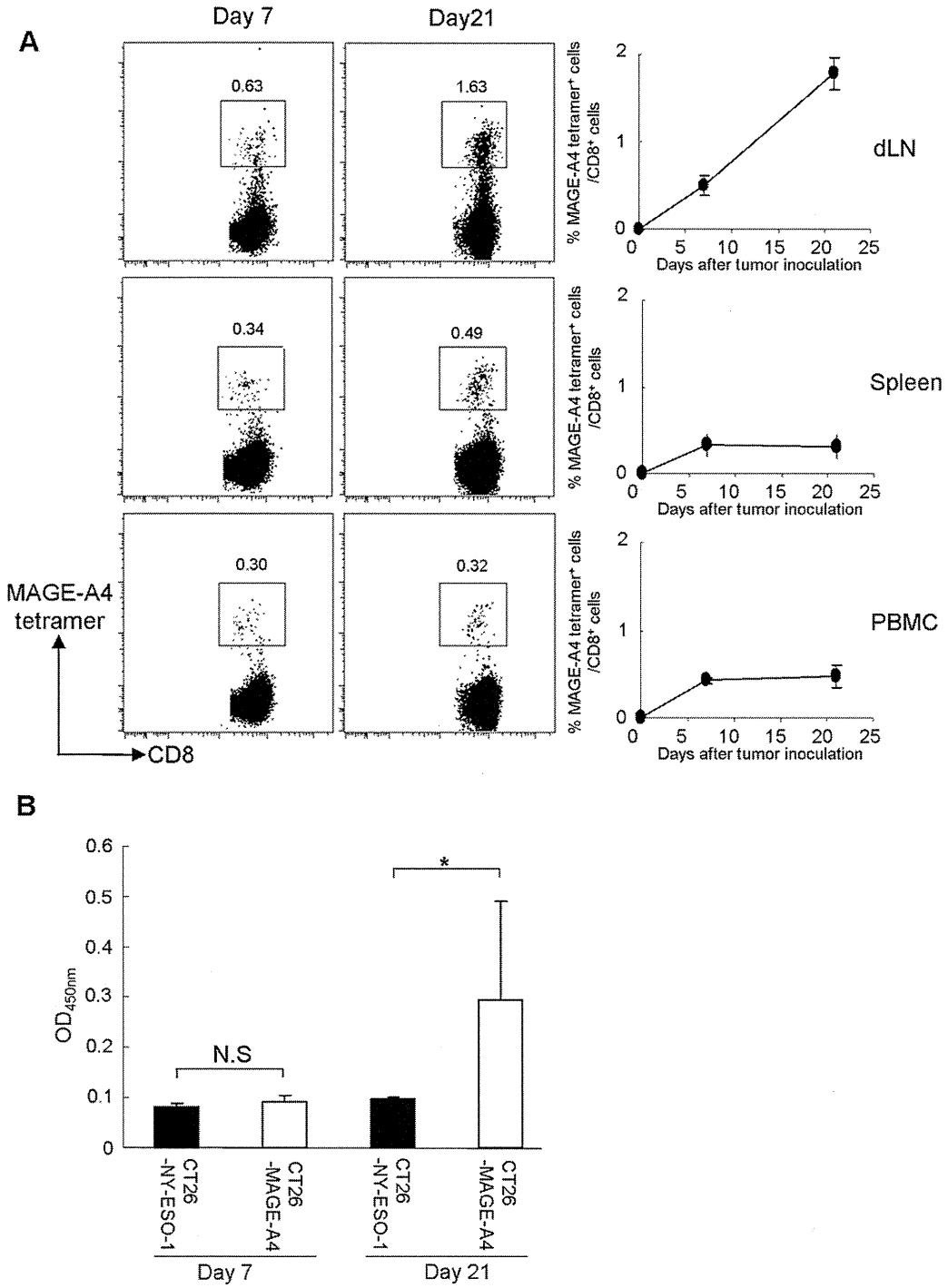

Fig. 6. Spontaneous MAGE-A4-specific CD8$^+$ T cells are primed after tumor inoculation. BALB/c mice were inoculated with CT26-MAGE-A4. (A) CD8$^+$ T cells were isolated from the draining lymph nodes (dLNs), spleens and PBMCs on the indicated days, and MAGE-A4-specific T cells was analyzed with MHC/peptide tetramer assay. (B) Sera were obtained on the indicated days, and Ab responses against MAGE-A4 were analyzed with ELISA. These experiments were repeated twice with similar results. Data are mean ± SD. *$p < 0.05$ as compared to control.

lymph nodes, spleens and PBMCs, but also tumor local sites. Our models could be valuable tools for analyzing antigen-specific T cells in both novel cancer immunotherapy and cancer immunotherapy that have been already tested in humans.

In our models, we found that spontaneous CD8$^+$ T cell and Ab responses were primed and increased along with tumor progression in both NY-ESO-1 and MAGE-A4 models [3,9]. Accumulating data show that induction/augmentation of anti-tumor immune responses are often detected in patients with larger tumors [3,14], suggesting that immune responses found in our NY-ESO-1 and MAGE-A4 tumor models closely parallel NY-ESO-1 and MAGE-A4 immune responses in humans. It has been a long debate whether spontaneous anti-tumor responses detected in cancer patients impact on tumor growth, as tumors continuously grow in patients harboring spontaneous anti-tumor immune responses. Our tumor model provides a clear answer for this conundrum. Although the immune responses spontaneously primed in tumor-bearing hosts partly inhibit a tumor growth, this immune response

is not strong enough to completely reject the tumor in the host. This means that further activation of immune responses by appropriate immunotherapy is essential for tumor rejection. Indeed, when these spontaneous immune responses were augmented by DNA vaccine, tumor growth was significantly inhibited. In contrast, we have reported that peptide vaccine using this NY-ESO-1 peptide enhanced tumor growth rather than inhibiting tumor growth unless it is vaccinated with proper adjuvants [13].

In fact, antigen-specific antibody may not play an important role for tumor rejection in our models, because 1) most tumor antigens including NY-ESO-1 and MAGE-A4 focused on this study, was exclusively expressed intracellularly by the tumor cells, thus not accessible for antibody [3] and 2) Ab responses were detected on day 21, namely later than $CD8^+$ T cell responses. Nevertheless, we have reported that injection of NY-ESO-1 mAb with chemotherapy, that can accentuate the release of intracellular tumor antigens to facilitate mAb access to intracellular target molecules, augmented anti-tumor effect in the same model system, though Ab administration alone did not inhibit tumor growth [18]. In our mouse model, spontaneously-primed anti-NY-ESO-1 Ab was detected when tumors reached a larger size. The level of spontaneously-primed antibody was, however, about 10-times lower than that achieved by mAb injection [18], suggesting that spontaneously-primed Ab responses may potentially have some anti-tumor effects, but the amount of Abs is too low to exhibit effective anti-tumor activity.

Since no NY-ESO-1 homologue is present in mice, the detected immune responses against NY-ESO-1 are considered to reflect a foreign antigen, rather than a self-antigen [3]. Whereas cancer-testis antigens like NY-ESO-1 are only expressed by cancer cells and testis, but not by normal somatic cells, mimicking foreign antigens, some cancer-testis antigens are reportedly expressed in medullary thymic epithelial cells under control of AIRE (Autoimmune regulator) [3,19]. It is plausible that cancer-testis antigens like NY-ESO-1 could be considered self-antigens during thymic selection, resulting in a repertoire of NY-ESO-1-specific T cells that are either subject to central or peripheral tolerance [3,20–22]. Thus, studies using mice in which NY-ESO-1 is a self-antigen should allow resolving this issue.

A unique finding of our study is that NY-ESO-1-specific $CD8^+$ T cell epitopes were present in an immunogenic part defined in humans [3]. This finding implies that immunogenicity may be characterized with similar components between humans and mice, further supporting the usefulness of our models. Our animal models provide important tools for the development of effective cancer vaccines.

In conclusion, we established animal models involving human tumor antigens, such as NY-ESO-1 or MAGE-A4 protein. These models allowed us to study the kinetics and distribution of antigen-specific immune responses in detail, and hence providing tools to optimize the efficacy of current cancer immunotherapy.

Acknowledgments

This article is dedicated to the memory of Lloyd J. Old, M.D. We thank Dr. J. Wing for critical reading and Ms. K. Mori and K. Sasada for excellent technical assistance.

This study was supported by Grants-in-Aid for Scientific Research (B) (HN) and Grants-in-Aid for Scientific Research on Priority Areas (HN and HS) from the Ministry of Education, Culture, Sports, Science and Technology of Japan, the Cancer Research Institute Investigator Award (HN). Cancer Research Grant from Foundation of Cancer Research Promotion (HN), the Sagawa Foundation for Promotion of Cancer Research (HN) and Senri Life Science Foundation (HN).

Contributions: Designed the experiments: DM, HN, TK, HS. Performed the experiments: DM, HN, TN, LW, ES. Analyzed the data: DM, HN, NH, TK, HS. Contributed reagents/materials/analysis tools: IL, EN. Wrote the paper: DM, HN, TK. *Conflicts of interest:* D.M. and N.H. are employees of ImmunoFrontier, Inc. The other authors have no potential conflicts of interest.

Appendix A. Supplementary data

Supplementary data associated with this article can be found, in the online version, at http://dx.doi.org/10.1016/j.vaccine.2013.02.056.

References

[1] Scanlan MJ, Gure AO, Jungbluth AA, Old LJ, Chen Y-T. Cancer/testis antigens: an expanding family of targets for cancer immunotherapy. Immunol Rev 2002;188:22–32.
[2] Boon T, Coulie PG, Van den Eynde BJ, Human van der Bruggen P. T cell responses against melanoma. Annu Rev Immunol 2006;24:175–208.
[3] Gnjatic S, Nishikawa H, Jungbluth AA, Gure AO, Ritter G, Jager E, et al. NY-ESO-1: review of an immunogenic tumor antigen. Adv Cancer Res 2006;95:1–30.
[4] Belardelli F, Ferrantini M, Parmiani G, Schlom J, Garaci E. International meeting on cancer vaccines: how can we enhance efficacy of therapeutic vaccines? Cancer Res 2004;64(18):6827–30.
[5] Rosenberg SA, Yang JC, Restifo NP. Cancer immunotherapy: moving beyond current vaccines. Nat Med 2004;10(9):909–15.
[6] Chen Y-T, Scanlan MJ, Sahin U, Tureci O, Gure AO, Tsang S, et al. A testicular antigen aberrantly expressed in human cancers detected by autologous antibody screening. Proc Natl Acad Sci USA 1997;94(5):1914–8.
[7] De Plaen E, De Backer O, Arnaud D, Bonjean B, Chomez P, Martelange V, et al. A new family of mouse genes homologous to the human MAGE genes. Genomics 1999;55(2):176–84.
[8] Duffour MT, Chaux P, Lurquin C, Cornelis G, Boon T, van der Bruggen P. A MAGE-A4 peptide presented by HLA-A2 is recognized by cytolytic T lymphocytes. Eur J Immunol 1999;29(10):3329–37.
[9] Miyahara Y, Naota H, Wang L, Hiasa A, Goto M, Watanabe M, et al. Determination of cellularly processed HLA-A2402-restricted novel CTL epitopes derived from two cancer germ line genes, MAGE-A4 and SAGE. Clin Cancer Res 2005;11(15):5581–9.
[10] Nishikawa H, Tanida K, Ikeda H, Sakakura M, Miyahara Y, Aota T, et al. Role of SEREX-defined immunogenic wild-type cellular molecules in the development of tumor-specific immunity. Proc Natl Acad Sci USA 2001;98(25):14571–6.
[11] Nishikawa H, Sato E, Briones G, Chen LM, Matsuo M, Nagata Y, et al. In vivo antigen delivery by a *Salmonella typhimurium* type III secretion system for therapeutic cancer vaccines. J Clin Invest 2006;116(7):1946–54.
[12] Griswold DP, Corbett TH. A colon tumor model for anticancer agent evaluation. Cancer 1975;36(6 Suppl):2441–4.
[13] Muraoka D, Kato T, Wang LA, Maeda Y, Noguchi T, Harada N, et al. Peptide vaccine induces enhanced tumor growth associated with apoptosis induction in $CD8^+$ T cells. J Immunol 2010;185(6):3768–76.
[14] Jager E, Stockert E, Zidianakis Z, Chen Y-T, Karbach J, Jager D, et al. Humoral immune responses of cancer patients against Cancer-Testis antigen NY-ESO-1: Correlation with clinical events. Int J Cancer 1999;84(5):506–10.
[15] Nishikawa H, Sakaguchi S. Regulatory T cells in tumor immunity. Int J Cancer 2010;127(4):759–67.
[16] Curiel TJ, Coukos G, Zou L, Alvarez X, Cheng P, Mottram P, et al. Specific recruitment of regulatory T cells in ovarian carcinoma fosters immune privilege and predicts reduced survival. Nat Med 2004;10(9):942–9.
[17] Sato E, Olson SH, Ahn J, Bundy B, Nishikawa H, Qian F, et al. Intraepithelial $CD8^+$ tumor-infiltrating lymphocytes and a high $CD8^+$/regulatory T cell ratio are associated with favorable prognosis in ovarian cancer. Proc Natl Acad Sci USA 2005;102(51):18538–43.
[18] Noguchi T, Kato T, Wang LN, Maeda Y, Ikeda H, Sato E, et al. Intracellular tumor-associated antigens represent effective targets for passive immunotherapy. Cancer Res 2012;72(7):1672–82.
[19] Gotter J, Brors B, Hergenhahn M, Kyewski B. Medullary epithelial cells of the human thymus express a highly diverse selection of tissue-specific genes colocalized in chromosomal clusters. J Exp Med 2004;199(2):155–66.
[20] Danke NA, Koelle DM, Yee C, Beheray S, Kwok WW. Autoreactive T cells in healthy individuals. J Immunol 2004;172(10):5967–72.
[21] Nishikawa H, Jager E, Ritter G, Old LJ, Gnjatic S. $CD4^+CD25^+$ regulatory T cells control the induction of antigen-specific $CD4^+$ helper T cell responses in cancer patients. Blood 2005;106:1008–11.
[22] Nishikawa H, Qian F, Tsuji T, Ritter G, Old LJ, Gnjatic S, et al. Influence of $CD4^+CD25^+$ regulatory T cells on low/high-avidity $CD4^+$ T cells following peptide vaccination. J Immunol 2006;176(10):6340–6.

Neuro-Oncology 15(6):747–758, 2013.
doi:10.1093/neuonc/not007
Advance Access publication March 3, 2013

NEURO-ONCOLOGY

Adoptive transfer of genetically modified Wilms' tumor 1–specific T cells in a novel malignant skull base meningioma model

Kenichiro Iwami, Atsushi Natsume, Masasuke Ohno, Hiroaki Ikeda, Junichi Mineno, Ikuei Nukaya, Sachiko Okamoto, Hiroshi Fujiwara, Masaki Yasukawa, Hiroshi Shiku, and Toshihiko Wakabayashi

Department of Neurosurgery, Nagoya University, Graduate School of Medicine, Nagoya, Aichi, Japan (K.I., A.N., M.O., T.W.); Department of Immuno-Gene Therapy, Mie University Graduate School of Medicine, Tsu, Mie, Japan (H.I., H.S.); Center for Cell and Gene Therapy, Takara Bio Inc., Otsu, Shiga, Japan (J.M., I.N., S.O.); Department of Bioregulatory Medicine, Ehime University Graduate School of Medicine, Matsuyama, Ehime, Japan (H.F., M.Y.)

Background. Meningiomas are the most commonly diagnosed primary intracranial neoplasms. Despite significant advances in modern therapies, the management of malignant meningioma and skull base meningioma remains a challenge. Thus, the development of new treatment modalities is urgently needed for these difficult-to-treat meningiomas. The goal of this study was to investigate the potential of build-in short interfering RNA-based Wilms' tumor protein (WT1)–targeted adoptive immunotherapy in a reproducible mouse model of malignant skull base meningioma that we recently established.

Methods. We compared *WT1* mRNA expression in human meningioma tissues and gliomas by quantitative real-time reverse-transcription polymerase chain reaction. Human malignant meningioma cells (IOMM-Lee cells) were labeled with green fluorescent protein (GFP) and implanted at the skull base of immunodeficient mice by using the postglenoid foramen injection (PGFi) technique. The animals were sacrificed at specific time points for analysis of tumor formation. Two groups of animals received adoptive immunotherapy with control peripheral blood mononuclear cells (PBMCs) or WT1-targeted PBMCs.

Results. High levels of *WT1* mRNA expression were observed in many meningioma tissues and all meningioma cell lines. IOMM-Lee-GFP cells were successfully implanted using the PGFi technique, and malignant skull base meningiomas were induced in all mice. The systemically delivered WT1-targeted PBMCs infiltrated skull base meningiomas and significantly delayed tumor growth and increased survival time.

Conclusions. We have established a reproducible mouse model of malignant skull base meningioma. WT1-targeted adoptive immunotherapy appears to be a promising approach for the treatment of difficult-to-treat meningiomas.

Keywords: adoptive immunotherapy, cranial nerve, skull base meningioma, Wilms' tumor 1.

Recent advances in T cell immunology and gene transfer have enabled adoptive tumor immunotherapy using genetically engineered T cells in clinical medicine.[1] Among a number of tumor-associated antigens, Wilms' tumor gene product 1 (WT1) is one of the most promising and universal target antigens for tumor immunotherapy. WT1-peptide vaccines have been the most widely evaluated, because they are easy to produce and are well tolerated in clinical trials with minimal toxicity.[2,3] However, whether vaccine therapies induce sufficient amounts of effector cells to kill solid tumors in vivo is an issue that remains to be addressed. In contrast, the adoptive transfer of ex vivo–expanded effector cells could be more advantageous than vaccination, given the greater control of tumor-specific effector cell numbers. Thus, adoptive T cell immunotherapy using WT1-specific T cell receptor (TCR) gene transfer is an alternative direct approach. To increase the effectiveness of TCR gene therapy, we have recently developed a novel vector system that can selectively express target antigen–specific TCR, in

Received June 13, 2012; accepted January 10, 2013.

Corresponding Author: Atsushi Natsume, MD, PhD, Department of Neurosurgery, Nagoya University, Graduate School of Medicine, 65, Tsurumai-cho, Showa-ku, Nagoya 466-8550, Japan (anatsume@med.nagoya-u.ac.jp).

which expression of endogenous TCR is suppressed by built-in short-interfering RNAs (siRNAs), named as siTCR vector.[4] By using this siTCR vector, we previously generated WT1-specific/HLA-A*2402–restricted T cells with enhanced antitumor cytotoxicity.[4,5]

Meningiomas are the most commonly diagnosed of all primary intracranial neoplasms, constituting ~30% of all primary tumors (Central Brain Tumor Registry of the United States, 2010). Approximately 75% of meningiomas are benign (World Health Organization [WHO] grade I), 20%–35% are atypical (WHO grade II), and 1%–3% are anaplastic/malignant (WHO grade III).[6,7] Despite significant advances in modern therapies, surgical resection remains the treatment of choice for many patients with meningiomas.[8–10] However, some histologically benign meningiomas often recur and become difficult to treat.[11] Moreover, grade II and III meningiomas have high recurrence rates after surgical or radiosurgical management.[12–14] In addition to the intrinsic biology, tumor location is also an important determinant of patient outcome. Skull base is a common site of origin for meningiomas. Complete resection of skull base meningioma is often not possible without a high risk of morbidity and mortality, given its surgical inaccessibility and proximity to vital brain structures, such as the cranial nerves. Cranial nerves are delicate nerves that arise directly from the brain, and meningiomas have a tendency to involve and infiltrate cranial nerves.[15] The management of malignant meningioma and skull base meningioma remains a challenge, and development of new treatment modalities is urgently needed for these difficult-to-treat meningiomas.

In this study, we examined the expression of WT1 antigen in meningioma tissues and found a high level of *WT1* mRNA expression in a majority of the tissues, compared with malignant gliomas. The evidence prompted us to develop adoptive transfer of WT1-specific TCR gene-engineered T cells targeting meningioma cells. In vitro studies revealed that TCR-transduced peripheral blood mononuclear cells (PBMCs) were able to secrete interferon-γ (IFN-γ) and lyse meningioma cells in an HLA-A*2402–restricted manner. To evaluate the efficacy of adoptive transfer of TCR-transduced PBMCs in meningioma in vivo, we developed a clinically relevant skull base model of malignant meningioma encasing the trigeminal nerve using the postglenoid foramen injection (PGFi) technique. To the best of our knowledge, this is the first report to describe the efficacy of adoptive immunotherapy by using genetically modified WT1-specific PBMCs in a meningioma model.

Materials and Methods

PBMCs

Whole blood samples were obtained from healthy donors who gave their informed consent. Whole blood was then diluted with the equal volume of phosphate-buffered saline (PBS) and FICOLL and centrifuged at 1600 rpm for 30 min. The buffy coat with PBMCs was carefully aspired. PBMCs were cultured in GT-T503 (Takara Bio, Shiga, Japan) supplemented with 1% autologous plasma, 0.2% human serum albumin, 2.5 mg/mL fungizone (Bristol-Myers Squibb, Tokyo, Japan), and 600 IU/mL interleukin-2 (IL-2). PBMCs obtained from the same donor and same blood sample were used to generate gene-modified PBMCs (GMCs) and non–gene-modified PBMCs (NGMCs).

Construction of Retroviral Vector and Retroviral Transduction

TCR genes were cloned from the HLA-A*2402–restricted $WT1_{235-243}$–specific $CD8^+$ CTL clone TAK-1.[16–18] Partial codon optimization was performed by replacing the C_α and C_β regions with codon-optimized TCR C_α and C_β regions, respectively.[4] Partially codon-optimized TCR-α and TCR-β genes were integrated into a novel vector encoding small-hairpin RNAs that complementarily bind to the constant regions of endogenous TCR-α and TCR-β genes (WT1-siTCR vector).[4]

PBMCs were stimulated with 30 ng/mL OKT-3 (Janssen Pharmaceutical, Beerse, Belgium) and 600 IU/mL IL-2 and transduced using the RetroNectin-Bound Virus Infection Method, in which retroviral solutions were preloaded onto plates coated with RetroNectin (Takara Bio), centrifuged at 2000 × *g* for 2 h, and rinsed with PBS. The procedure was repeated twice on days 4 and 5 after the initiation of PBMC culture. PBMCs were applied onto the preloaded plate.[4] The transduced PBMCs were cultured for a total of 10 days. Control PBMCs (NGMCs) and TCR-transduced PBMCs (GMCs) were stored frozen in liquid nitrogen, thawed, and cultured in GT-T503 supplemented with 1% autologous plasma, 0.2% human serum albumin, 2.5 mg/mL fungizone, and 600 IU/mL IL-2 for 2 days to use in all the experiments below.

Cell Lines

The human meningioma cell lines IOMM-Lee (HLA-A*2402/0301),[19] HKBMM (HLA-A*2402/1101),[20] and KT21-MG1 (HLA-A*0207/1101)[21] were used. IOMM-Lee was kindly provided by Dr. Anita Lai (University of California at San Francisco, CA), and HKBMM and KT21-MG1 were from Dr. Shinichi Miyatake (Osaka Medical University, Osaka, Japan). The T2A24 cell line was derived from the T2 cell line, which is deficient in TAP transporter proteins, after transfection with the HLA-A*2402 complementary DNA (cDNA). The human embryonic kidney cell line GP2-293 was obtained from the American Type Tissue Culture Collection (ATCC; MD). All cell lines were maintained in Dulbecco's modified Eagle's medium containing 10% fetal bovine serum and penicillin/streptomycin. Cell lines were grown at 37°C in a humidified atmosphere of 5% carbon dioxide. HLA-A genotyping was performed using polymerase chain reaction (PCR) sequence-based typing (SRL, Tokyo, Japan).

Sample Collection and RNA Extraction

Tumor specimens for molecular genetic analysis were obtained from 29 patients with meningioma and 25 patients with high-grade glioma who underwent surgical procedures at Nagoya University Hospital or affiliated hospitals. The molecular genetic analysis performed in this study was approved by the institutional ethics committee of Nagoya University, and all patients who registered for this study provided written informed consent. All tumors were histologically verified according to the WHO 2007 guidelines; 23 patients had grade-I meningioma, 5 had grade-II meningioma, 1 had grade-III meningioma, 6 had grade-III glioma, and 19 had grade-IV glioma. RNA purification was performed using the standard TRIzol (Invitrogen, Carlsbad, CA) method.

Quantitative Analysis of WT1 mRNA Expression

Total RNA was extracted from 54 tumors, 3 cell lines, and normal whole brain (Human Total RNA Master Panel II; Takara Bio, Otsu, Japan), and first-strand cDNA was synthesized using the Transcriptor First Strand cDNA Synthesis Kit (Roche, Mannheim, Germany). The cDNA product was used in reverse-transcription (RT) PCR for the quantitation of *WT1* and *GAPDH* mRNA levels. The primers and Taqman probes for the assay were purchased from Roche Diagnostics (Indianapolis, IN). The sequences of the primers and probe used to detect *WT1* mRNA were as follows: WT1 forward primer (5′-GATAACCACAC AACGCCCATC-3′), WT1 reverse primer (5′-CACACG TCGCACATCCTGAAT-3′), and WT1 probe (5′-FAM-ACACCGTGCGTGTGTATTCTGTATTGG-TAMRA-3′). The sequences of the primers used to detect *GAPDH* mRNA were as follows: GAPDH forward primer (5′-AGCCA CATCGCTCAGACAC-3′) and GAPDH reverse primer (5′-GCCCAATACGACCAAATCC-3′). The GAPDH probe was from the Roche Human Probe Library (no. 60). RT-PCR assay was performed using the LightCycler 480 Probes Master and LightCycler 480 instrument II (Roche Diagnostics). *WT1* expression was normalized to that of *GAPDH* in each sample.

Measurement of Proviral Copy Number in Retrovirus-Transduced PBMCs

Genomic DNA was purified from transduced PBMCs, and the mean proviral copy number per cell was quantified using the Cycleave PCR core kit (Takara Bio) and Proviral Copy Number Detection Primer Set (Takara Bio).

Flow Cytometry

PE-conjugated anti-human CD4 monoclonal antibody (mAb; eBioscience, San Diego, CA), FITC-conjugated anti-human CD8 mAb (BD Biosciences, San Diego, CA), and PE-conjugated $WT1_{235-243}$/HLA-A*2402 tetramer (provided by Dr. Kuzushima, Aichi Cancer Center Research Institute) were used. Stained cells were analyzed using a FACScanto II flow cytometer (BD Biosciences).

For intracellular IFN-γ staining, PBMCs (1.0×10^6 cells) were cultured with IOMM-Lee or KT21-MG1 meningioma cells (1.0×10^6 cells) for 1 h. BD GolgiStop (0.7 μg/mL; BD Biosciences) was added, and cells were cultured for an additional 8 h. Then, the PBMCs were incubated with Fc blocker (eBioscience, San Diego, CA) and stained with FITC-conjugated anti-human CD8 mAb. After this, the PBMCs were incubated with BD Cytofix/Cytoperm solution (BD Biosciences) at 4°C for 20 min and then washed with BD Perm/Wash solution (BD Biosciences). The PBMCs were then incubated with APC-conjugated anti-human IFN-γ mAb (BD Biosciences), followed by flow cytometry.

Calcein-AM Cytotoxicity Assay

The ability of the transduced PBMCs to lyse target cells was measured using a calcein-AM (Dojindo, Kumamoto, Japan) release assay, as described previously.[22] In brief, 5×10^3 calcein-AM–labeled target cells and various numbers of effector cells in 200 μL of RPMI 1640 medium containing 10% fetal bovine serum were seeded into 96-well round-bottom plates. The target cells were incubated with or without 10 nM WT1 peptide for 2 h before the addition of effector cells. After incubation with the effector cells for 4 h, 100 μL of supernatant was collected from each well. The percentage of specific lysis was calculated according to the formula [(experimental release – spontaneous release)/(maximum release – spontaneous release)] × 100.

Generation of Green Fluorescent Protein–Expressing IOMM-Lee Cells

A retrovirus expressing green fluorescent protein (GFP) was constructed using the Retro-X Universal Packaging System (Clontech, CA). GP2-293 cells were transfected with pRetroQ-AcGFP-C1 along with a pVSVG plasmid (Clontech). After 48 h, cell-free viral supernatants were obtained and stored at −80°C. IOMM-Lee cells were transduced with the retroviral vectors encoding GFP with use of the RetroNectin-bound Virus Infection Method, in which retroviral solutions were preloaded onto RetroNectin-coated plates, centrifuged at 2000 × *g* for 2 h, and rinsed with PBS. IOMM-Lee cells were then applied onto the preloaded plate.

Skull Base Meningioma Xenograft

NOD/Shi-SCID, IL-2Rγ_c^{null} (NOG) mice were created at the Central Institute of Experimental Animals (Kawasaki, Japan) by backcrossing γ_c^{null} mice with NOD/Shi-SCID mice, as reported previously.[23] Eight-week-old mice were given intracranial injections containing 3 μL of 5.0×10^4 freshly dissociated GFP-expressing IOMM-Lee cells with use of the PGFi technique.[24] In brief, the mice were anesthetized with

an intraperitoneal injection of 45 mg/kg sodium pentobarbital (Dainippon Sumitomo Pharma, Osaka, Japan). A 26-gauge needle tip was positioned on the right PGF (the rostral area of the opening of the external acoustic meatus). The implantation site, the lateral part of the foramen ovale, was accessed via the following injection track: horizontal angle, 60°; sagittal angle, −45°; and insertion depth, 3 mm (Supplementary Material, Fig. S1A and B). The cells were injected over 5 s. The needle was slowly withdrawn over several seconds. Minimal finger pressure was applied for 30 s after needle withdrawal to stop the bleeding at the puncture site. After the injections, the mice were given free access to water and were examined twice per day. Corneal sensitivity was also recorded using a cotton filament, and the blinking of the right eye was compared with that of the control (left) eye.

In Vivo Anti-Meningioma Effects of WT1-siTCR Gene-Transduced CTLs

In our preliminary experiments, the median survival of untreated animals was consistently 12.5 days (data not shown). Twenty-four mice bearing established tumors were randomly assigned to 2 different experimental groups. Five days after tumor inoculation, human PBMCs (5.0×10^7 cells) were injected into the tail vein. On the twelfth day after tumor inoculation, 6 mice per group were sacrificed to evaluate tumor size and $CD8^+$ T cell infiltration. According to statistical considerations based on our preliminary experiments, the remaining mice were monitored for signs of keratopathy and survival for up to 28 days after inoculation,

Tissue Processing and Immunohistochemistry

Mouse heads were fixed in 10% neutral buffered formalin (Wako Pure Chemical Industries, Osaka, Japan) for 48 h. GFP fluorescence in tumor cells was analyzed using a fluorescence imaging system (IVIS spectrum; Caliper Life Sciences, Alameda, CA) after the removal of the skull. Two-dimensional tumor size was calculated from the fluorescent area by using the Living Image software (Caliper Life Sciences), because the established tumors grew in a flattened pattern, similar to meningioma en plaque in humans. For histopathologic examination, formalin-fixed mouse heads were decalcified in Decalcifying Solution B (Wako Pure Chemical Industries) for 96 h and embedded in paraffin. Serial 5-μm sections were cut and processed for hematoxylin and eosin (H&E) staining, Luxol fast blue (LFB) staining, or immunohistochemistry. The sections were deparaffinized with xylene and rehydrated with ethanol. LFB staining was performed according to the method of Werner et al.[25] In brief, the sections were placed in 0.1% LFB solution at 60°C for 16 h. After several washes, sections were differentiated in 0.05% lithium carbonate solution, followed by 70% ethanol. The slides were then incubated in 0.1% Cresyl echt violet solution to counterstain nuclei. Immunohistochemistry for human $CD8^+$ T cells was performed using anti-human CD8 antibody (MBL, Nagoya, Japan). In brief, the sections were rinsed in PBS and incubated with the antibody freshly diluted at 1:100 in PBS. The Vector M.O.M. Immunodetection Kit (Vector Laboratories, Burlingame, CA) was used to perform the secondary antibody incubations. The staining was visualized with diaminobenzidine, and sections were counterstained with hematoxylin. We counted the number of both normal tissue-infiltrating (oral mucosa and submucosal soft tissues) and tumor-infiltrating $CD8^+$ T cells in a microscopic grid 0.5 × 0.5 mm in size (0.25 mm^2) at a magnification of 200×. The area with the most abundant distribution of $CD8^+$ T cells was selected in each mouse.

Statistical Analysis

Comparisons between groups were done using paired *t* test or Welch's *t* test or Mann–Whitney exact test, where appropriate. Differences were considered to be statistically significant at $P < .05$. The outliers were defined as data points that were >3 times the interquartile ranges below the first quartile or above the third quartile. The Kaplan-Meier method and log-rank test were used to determine whether there was a significant difference in clinical events between the groups.

Results

WT1 *Expression in Meningioma Patient Samples and Cell Lines*

WT1 mRNA levels in samples from patients with meningioma and human meningioma cell lines were determined using quantitative RT-PCR and calculated relative to the WT1 expression level in the normal brain. As shown in Table 1, *WT1* mRNA was expressed at high levels in samples from patients with meningioma. Of interest, a correlation was found between the *WT1* expression levels and the MIB-1 labeling index ($P = .0018$, Fig. 1A), but there was no significant correlation with tumor location, tumor grading, and performance status (modified Rankin scale). We also examined *WT1* expression in 25 high-grade glioma samples. The mean expression level of *WT1* mRNA in meningioma samples was significantly higher than that in high-grade glioma samples (26.25 [18.27] vs. 5.45 [12.52]; $P = .000014$). The genotype, *WT1* expression levels, and intracranial tumorigenicity of NOG mice implanted with the 3 meningioma cell lines are presented in Table 2. In all the 3 meningioma cell lines, the *WT1* mRNA levels were >8-fold higher than that of the normal brain.

Cell Surface Expression of CD4, CD8, and WT1-Specific TCR in NGMCs and GMCs

PBMCs were transduced with WT1-siTCR at relatively low copy numbers to reduce the risk of insertional

Table 1. Data on patients with meningiomas and tumor characteristics

	Age (years)/ Sex	Location of Lesion	Pathological Diagnosis (subtype)	WHO Grade	MIB-1 Index (%)	Relative Quantity of WT1 mRNA (NB = 1)	Extent of Resection (Simpson grade)	Follow-up Period (month)	Recurrence/ Regrowth	mRS
1	71M	SB	meningothelial	I	ND	19.43	2	39	−	0
2	49F	non- SB	meningothelial	I	ND	5.06	2	55	−	0
3	69F	non- SB	fibrous	I	ND	27.86	3	77	−	0
4	68F	non- SB	transitional	I	ND	22.78	1	77	−	0
5	30F	SB	meningothelial	I	ND	25.63	2	23	−	1
6	68M	SB	meningothelial	I	ND	12.64	4	15	−	5
7	73F	SB	meningothelial	I	ND	20.68	2	32	−	1
8	46F	SB	meningothelial	I	<1	7.78	2	76	−	0
9	36F	SB	meningothelial	I	ND	22.63	2	65	−	1
10	64M	SB	meningothelial	I	ND	12.55	2	7	−	2
11	56M	non- SB	fibrous	I	ND	48.17	1	57	−	0
12	46F	non- SB	meningothelial	I	ND	56.89	1	69	−	0
13	42F	non-s SB	meningothelial	I	ND	4.50	1	89	−	2
14	58M	SB	meningothelial	I	5	38.59	2	65	+	1
15	39F	non- SB	transitional	I	3	39.67	1	2	−	3
16	72F	non- SB	fibrous	II	3	33.13	2	72	+	1
17	63M	SB	atypical	II	4	60.97	4	63	−	1
18	77M	SB	meningothelial	I	1–2	4.03	4	70	−	0
19	54M	SB	meningothelial	I	1–3	7.57	4	53	−	2
20	33F	non- SB	meningothelial	II	5–6	47.50	4	16	−	2
21	48F	SB	meningothelial	I	ND	28.25	2	57	−	1
22	62M	SB	meningothelial	I	ND	47.84	4	2	−	1
23	66F	SB	meningothelial	II	ND	58.49	1	48	−	2
24	70F	SB	atypical	II	20–30	41.64	2	80	+	1
25	52M	SB	atypical	II	10–15	14.22	3	37	+	5
26	55M	SB	atypical	II	2	4.63	2	73	−	1
27	63M	non- SB	atypical	II	4	2.79	2	83	−	0
28	45M	non- SB	clear cell	II	1–2	9.06	1	92	−	0
29	68F	non- SB	anaplastic	III	3–10	36.25	3	64	+	2

Abbreviations: mRS, modified Rankin Scale; NB, normal brain; ND, not done; SB, skull base.

mutagenesis. In the GMCs used in this study, the proviral copy number was 2.24 copies per cell (data not shown). $CD4^+$ and $CD8^+$ cells constituted 14.6% and 78.4% of NGMCs and 19.7% and 72.8% of GMCs, respectively (Fig. 1B). About 20% of the GMCs were positive for HLA-A*2402/WT1 tetramer staining (Fig. 1B). Moreover, HLA-A*2402/WT1-tetramer positivity in $CD3^+CD8^+$ cells and $CD3^+CD4^+$ cells was 36.2% and 36.3%, respectively, suggesting that both fractions were similarly transduced (Supplementary Material, Fig. S3A). These NGMCs and GMCs were used as effector cells in subsequent assays.

Intracellular IFN-γ Production by GMCs Against Human Meningioma Cell Lines

To confirm that the freezing and thawing procedures had not affected the antigen specificity and HLA restriction of GMCs, we first investigated their intracellular IFN-γ production in response to WT1-peptide–loaded and nonloaded T2A24 cells. As demonstrated previously, GMCs exhibited specific reactivity to WT1-peptide–pulsed T2A24 cells (data not shown).[4,5] We also investigated the intracellular IFN-γ production in NGMCs and GMCs against WT1-positive meningioma cell lines, KT21-MG1 (HLA-A*2402 negative) and IOMM-Lee (HLA-A*2402 positive). As shown in Fig. 1C, GMCs exhibited specific reactivity to IOMM-Lee cells. These data confirm that GMCs can recognize WT1-positive meningioma cells in an HLA-A*2402–restricted manner.

Cytotoxicity of GMCs Against Human Meningioma Cell Lines

To determine whether GMCs were able to lyse target cells, effector cells were mixed with calcein-AM–labeled target cells. As shown in Fig. 1D, GMCs lysed